AD_____

Award Number: DAMD17-02-1-0586

TITLE: Tumor-Secreted Autocrine Motility Factor (AMF): Casual Role in an Animal Model of Cachexia

PRINCIPAL INVESTIGATOR: John M. Chirgwin, Ph.D.

CONTRACTING ORGANIZATION: University of Virginia
Charlottesville, Virginia 22904

REPORT DATE: August 2004

TYPE OF REPORT: Annual

PREPARED FOR: U.S. Army Medical Research and Materiel Command
Fort Detrick, Maryland 21702-5012

REPORT DOCUMENTATION PAGE

Form Approved
OMB No. 074-0188

1. AGENCY USE ONLY (Leave blank)	2. REPORT DATE	3. REPORT TYPE AND DATES COVERED
	August 2004	Annual (1 Aug 2003 - 31 Jul 2004)

4. TITLE AND SUBTITLE
Tumor-Secreted Autocrine Motility Factor (AMF): Casual Role in an Animal Model of Cachexia

5. FUNDING NUMBERS
DAMD17-02-1-0586

6. AUTHOR(S)
John M. Chirgwin, Ph.D.

7. PERFORMING ORGANIZATION NAME(S) AND ADDRESS(ES)
University of Virginia
Charlottesville, Virginia 22904

Email = jc3qb@virginia.edu

8. PERFORMING ORGANIZATION REPORT NUMBER

9. SPONSORING / MONITORING AGENCY NAME(S) AND ADDRESS(ES)
U.S. Army Medical Research and Materiel Command
Fort Detrick, Maryland 21702-5012

10. SPONSORING / MONITORING AGENCY REPORT NUMBER

11. SUPPLEMENTARY NOTES

12a. DISTRIBUTION / AVAILABILITY STATEMENT
Approved for Public Release; Distribution Unlimited

12b. DISTRIBUTION CODE

13. Abstract ***(Maximum 200 Words)*** *(abstract should contain no proprietary or confidential information)* Cancer cachexia has three clinical features: 1) loss of appetite (anorexia), 2) nutritional mal-absorption, and 3) muscle and fat wasting caused by tumor-stimulated factors. This project focuses on muscle wastiung. A number of factors have been proposed to cause cancer cachexia. Lack of progress in the area is unfortunate, given the tremendous benefit patients with advanced cancer would receive from effective treatment of cachexia to improve quality of life and postpone mortality. We proposed that autocrine motility factor (AMF) is released into the bloodstream from cancer sites and stimulates muscle wasting. In the second grant period we have now demonstrated that administration of recombinant AMF protein to mice results in a statistically significant loss of weight, compared to control treatment, in 24 hours. We are ready to test the species specificity of this response. We have also determined the molecular structure of the recombinant mouse protein. In the next and final research year will assess some of the molecular pathways activated in muscle by AMF, which could contribute to cachexia. These include activation of proteasomal muscle protein degradation via the Foxo transcription factors and PI3 kinase pathways and alterations in the secreted regulators of muscle mass, IGF-1 and myostatin.

14. SUBJECT TERMS
cancer cachexia, proteasome, muscle wasting, phosphoglucose isomerase glucose 6-phosphate isomerase, autocrine motility factor

15. NUMBER OF PAGES
45

16. PRICE CODE

17. SECURITY CLASSIFICATION OF REPORT	18. SECURITY CLASSIFICATION OF THIS PAGE	19. SECURITY CLASSIFICATION OF ABSTRACT	20. LIMITATION OF ABSTRACT
Unclassified	Unclassified	Unclassified	Unlimited

Table of Contents

INTRODUCTION:

Update on cancer cachexia, August 2004. The previous (first annual) progress report provided an extensive update. We provide only information new since then. Substantial progress has been made to identify biochemical mechanisms leading to muscle wasting and atrophy, but there have been no substantive breakthroughs in development of new animal models of cachexia, identification of additional circulating factors responsible for the syndrome, or the development of novel patient treatments (Tisdale, 2003).

Biochemical mechanisms of cachexia have been explored in vivo and in vitro. It now appears that muscle wasting involves paracrine factors in the microenvironment surrounding muscle that regulate its overall activity, in particular insulin-like growth factor-1 (Glass, 2003) and the TGF-beta superfamily member myostatin, also known as GFD-8, which is a negative regulator of muscle mass. (Roth & Walsh, 2004). IGF-1 appears to stimulate the PI3 kinase/Akt signaling and Foxo transcription factor pathways (Lee et al, 2004; Stitt et al, 2004; Sandri et al, 2004). The same pathways appear to be activated during muscle wasting in response to multiple causes; so these are likely also to be activated during cancer-induced muscle wasting (Lecker et al, 2004). Myosin heavy chain is a major substrate for degradation in cachectic skeletal muscle (Acharyya et al, 2004).

Role of the proteasome. Skeletal muscle proteolysis in cachexia is probably due to increased activity through the proteasomal pathway, rather than via lysosomes or soluble sarcoplasmic proteases. Certain cancer treatments can either enhance or inhibit this muscle degradation pathway. Thus, cancer chemotherapy may alter cachexia in patients. Omega-3 fatty acids and other eicosanoids can regulate the activity of the proteasome, providing a biochemical rationale for the dietary treatment of cancer cachexia. It is not yet clear that activation of proteasomal degradation is the central or the only pathway for muscle wasting in cancer cachexia (Glass, 2003; Lecker, 2003), but this seems increasingly likely and may involve specific activation in muscle cells of the specific ubiquitin E3 ligases, atrogin and MuRF1 (Dehoux et al, 2004; Sachek et al, 2004) .

This report described progress on our project (now in its second year) to establish whether autocrine motility factor/phosphoglucose isomerase is a systemic cachectic factor. It has been known for 50 years to be elevated in patients with advanced, metastatic breast cancer, and we previously observed that it was also elevated in the circulation of nude mice that were cachectic due to advanced breast cancer metastases restricted to bone.

BODY OF PROGRESS REPORT

Timetable: The award of this grant was made just as the Principal Investigator was moving from the University of Texas to the University of Virginia. Initial work was commenced upon arrival in Charlottesville Virginia in October 2002. A new research associate was recruited to work on this project, Ms. Lisa Wessner, who has learned all of the techniques specific to the project, which has now been active since January 1 of 2003. Thus, this progress report represents work carried out over a 12 month period from July 2003 to July 2004, and the report ends after 18 months of research have been carried out in total. The animal results reported below, although gratifyingly successful, were substantially delayed by a serious, documented outbreak of the lethal mouse pathogen *Burkholderia gladioli* (Foley et al, 2004) in our animal facility. This caused two problems. *Burkholderia* can be easily transmitted from regular lab mouse strains to immunocompromised ones. Under our quarantine conditions, animal handlers can only handle nude mice if they have been completely decontaminated after handling non-nudes. This is highly impractical, since a central part of our research involves growth of human tumor cells in nude mice, typically in 6-month experiments. The only practical solution to this problem has been to carry out ALL animal experiments in nudes. Our ultimately successful quarantine approach was to avoid initiation of all new anima experiments, while the source of the outbreak was determined and infected animals were identified and sacrificed. This took six months. Our animal experiments, shown below, have thus been delayed by six months. For this reason we have requested a one-year no-cost extension of funding to permit us to complete the remaining tasks. Thus, we anticipate filling the final progress report for this proposal in August 2005.

The revised application contained **3 Specific Aims and 9 Tasks** in the revised Approved **Statement of Work**:(Revised 01/04/02 with original Aims 4 & 5 deleted):

Task 1 (Aim 1) Determine dose range and Alzet mini-pump size for administration of mAMF to achieve effective blood levels of ~10ng/mL. [28 mice] Year 01, months 1-6.

Task 2 (Aim 1) Demonstrate cachexia with mouse AMF infused into mice, compared to controls and to mice bearing CHO-K1 [mAMF-] and CHO-1C6 [mAMF+] IM tumors. [56 mice] Year 01, months 7-12.

Task 3 (Aim 1) Carry out routine pathology and histology of animals from Task 2. Year 01, months 10-12.

Task 4 (Aim 1) Determine host concentrations of 4 host cytokines in baseline and sacrifice blood samples of animals from task 2. Year 02, months 1-4.

Task 5 (Aim 2) Construct two mutants of mAMF [E357A and 4S/T-A] and sequence. Year 02, months 1-4.

Task 6 (Aim 2) Express and purify mutant mAMF proteins and determine Km and Vmax and binding to phosphocellulose. Year 02, months 5-8.

Task 7 (Aim 2) Carry out Task 2 & 3 protocols with wt & 2 mutant mAMFs by pump infusion. [24 mice] Year 01, months 9-2; Year 02, throughout.

Task 8 (Aim 3) Carry out Task 2 & 3 protocols with mouse versus 3 concentrations of human AMF. [40 mice] Year 02, months 1-12.

Task 9 (Aims 1-3) Analyze data, prepare and submit results for meeting presentations, progress reports, and peer-reviewed publication. Year 01-02, throughout.

Total mice requested = 148 [adult female Balb/c & Balb/c nudes, 32 mice were eliminated in deleted Aim 5]. All use of human cell lines and radioisotopes was eliminated with the deletion of Aims 4 & 5. Animal use has been reported separately to the DoD. Since the annual animal usage and progress reports cover different times, the most recent animal usage form did not include the mice that were used in Figures 1 and 2.

Progress:

Task 1 was completed in the first year.

Task 2 has been carried out in this report period. Previous experiments demonstrated that a simpler approach than originally proposed successfully gave substantially increased steady-state blood concentrations of mouse PGI/AMF. In this experimental protocol, animals were given the factor as sterile intraperitoneal (i.p.) injections of protein in PBS at 8 AM, noon, and 4 PM. Blood levels of PGI/AMF were measured at the 4PM time, and the animals were weighed. The injected mouse AMF/PGI was entirely cleared from the blood stream by 24 hours. **Figures 1 and 2** show the result of a substantial animal experiment in which nude mice were injected 3 time per day for 3 days with 100 µl of sterile PBS containing purified mouse AMF/PGI (positive, shown in square symbols) or BSA (negative control) at either 150 or 500 µg of protein per dose. The experiment was carried out with Balb/C nu/nu mice and 5 or 10 mice per group. Statistical significance was determined by analysis of variance using the 2-way ANOVA facility plus post-test analysis of the GraphPad Prizm graphics program. The data demonstrate that 150 µg doses were ineffective to cause weight loss (**Figure 1**), while 500 µg doses (**Figure 2**) caused a statistically highly significant cachexia by 24 hours after the initial injection, which appeared to persist for 24hrs after the cessation of injection following three days of treatment.

Mouse AMF/PGI for these experiments was prepared in E coli and purified by NiNTA chromatography using the 6xHis C-terminal extension. As detailed in the first progress report, these recombinant protein preparations were carefully analyzed for contamination with bacterial endotoxin and determined to be free of this material to well below a level that would cause inflammation in the animals. The laboratory animal personnel report that the AMF/PGI treatments did not cause any apparent pain or discomfort to the mice.

On the basis of the results shown in **Figures 1 and 2**, the experiments for **Tasks 3 and 4** will be carried out in the next funding period by direct i.p. injection of recombinant protein 3X per day at the dosage used for **Figure 2**. In addition to the routine histology proposed in task 3, we will assess whether a series of muscle genes are activated. Mice will be sacrificed at the end of the third day of treatment. Muscle RNA will be assayed by real-time PCR with mouse-

specific primer pairs for a series of markers discussed in the Introduction, above: IGF-1, myostatin, atrogin, MuRF-1, myosin heavy chain, and Foxo 3. We will also prepare muscle homogenates from treated and control mice and assay them for proteasomal activity (Reinheckel et al, 2000) as shown in **Figure 3**.

Tasks 5 and 6 have been completed. The catalytically inactive mutant E357A has been constructed, expressed and purified. In collaboration with Dr Christopher Davis at the University of South Carolina, the x-ray crystal structure of this mutant has been determined. The data were originally included in the manuscript submitted to J Mol Biol, now in press as Solomons et al (below under Research Accomplishments, but the data on the mutant were removewd to keep the paper within acceptable page limits and will be submitted later. The role of isomerase (PGI) activity in relation to autocrine motility factor (AMF) activity remains controversial in the field. Much of the published AMF cytokine work has not taken into account the current knowledge of PGI structure. We (Davies et al, 2003) and others (Arsenieva & Jefferey, 2002), have shown that ligand binding to mammalian PGIs results in only very small conformational changes in the surface of the protein away from the active site (where binding to the AMF receptor almost certainly takes place). These conformational changes are almost certainly insufficient to have any effect on a receptor-mediated cytokine-like action of the protein. We believe that mouse E357A AMF/PGI will be active in the cachexia assay. This is proposed in **Task 7**, which will be carried out in the final funding period.

We are also ready to carry out **Task 8**, the cachexia model, by injecting mice with 500 μg/dose of human AMF/PGI. Our extensive preliminary data, presented previously, showed an approximately 100-fold species preference for mouse versus human factor acting on cells of the same versus the opposite species. We thus expect that this dose of the human protein will be without effect. 100X higher should be effective, but it is impractical both for the investigator and the mouse to repeat the experiment with 50 mg of purified protein per dose.

KEY RESEARCH ACCOMPLISHMENTS:

1) Purification of recombinant AMF/PGI with low endotoxin content finalized.

2) Animal model of direct i.p. injection of mouse AMF/PGI established in previous year successfully used to cause statistically significant (4%) weight loss in 24hrs compared to equivalent control protein treatment. Partial dose-response established between 450 (ineffective) and 1500 (effective) μg/mouse/day.

3) Human AMF/PGI prepared to carry out species-specific test of the results found in accomplishment 2) in 3rd (final) year.

4) Crystal structure of mouse AMF/PGI, used in all of the work for this proposal, solved and published.

5) In vitro assay for proteasome activation in mouse C2C12 myoblasts established and responses to mouse AMF/PGI demonstrated.

REPORTABLE OUTCOMES (since previous report):

Six manuscripts published, which include reviews of the contributions of bone metastases to cancer cachexia, while the sixth paper derives directly form the work carried out for this proposal:

Chirgwin JM, Guise TA. Interactions between tumor and bone alter the phenotypes of both. J Musculoskel Neuronal Interact, 3:278-281, 2003.

Chirgwin JM, Guise TA. Molecular mechanisms of cancer metastases to bone. Curr Opin Orthop, 14:317-321, 2003.

Guise TA , Chirgwin JM. Role of TGFβ in osteolytic bone metastases. Clin Orthop, 415:S32-38, 2003.

Chirgwin JM, Guise TA. Cancer metastasis to bone. Science & Medicine, 9:140-151, 2003.

Chirgwin JM, Mohammad KS, Guise TA. Tumor-bone cellular interactions in skeletal metastases. J Musculoskeletal Neuronal Interact 4:308-318, 2004. Copy in appendix.

Graham Solomons JTG, Burns S, Wessner L, Krishnamurthy N, Zimmerly E, Swan MK, Krings S, Muirhead H, Chirgwin J, Davies C. The crystal structure of mouse phosphoglucose isomerase at 1.6 Å resolution and its complex with glucose 6-phosphate reveals the mechanism of sugar ring opening. J Mol Biol. 342:847-860, 2004. Copy in appendix.

Two manuscripts in press or accepted for publication, which include reviews of the contributions of bone metastases to cancer cachexia:

Guise TA, Chirgwin JM. Biology of bone metastases. Chapter in Diseases of the Breast, 3rd edition. Harris, Lippman, Morrow, and Osborne (eds). Lippincott Williams & Wilkins, in press, 2004.

Clines GR, Chirgwin JM, Guise TA. Skeletal complications of malignancy: central role of the osteoclast. Chapter for Topics in Bone Biology, Vol 2, accepted for publication, 2004.

CONCLUSIONS

Purified mouse autocrine motility factor/phosphoglucose isomerase was found to cause statistically weight loss (cachexia) after 3 days of 3X daily intraperitoneal injection at a dose of 0.5 mg/injection, which was accompanied by significant increases in serum concentrations of the factor. This is a simpler animal model than originally proposed. Thus, the main hypothesis of the original proposal has been validated.

Progress in the second year has been fully successful but substantially delayed by a disease outbreak in the P.I.'s animal facility. Experiments for 2004 were delayed until June and July. We have requested and received a one-year no cost extension of the grant from the DoD and now plan to complete the work proposed by the end of July 2005.

Structures of the AMF/PGI proteins, including mouse and human proteins and the enzyme complexed with inhibitor have been solved by x-ray crystallography and published or accepted for publication. Mutant forms of the protein have been prepared. Experiments have been successfully completed to improve the purity of the recombinant protein and to characterize the effects of the factor on both intact animals and on a mouse muscle cell line in vitro. The structural data are now complete for analysis of the species-specific effects and their structural bases

COMPREHENSIVE LIST OF REFERENCES:

Acharyya S, Ladner KJ, Nelsen LL, Damrauer J, Reiser PJ, Swoap S, Guttridge DC (2004). Cancer cachexia is regulated by selective targeting of skeletal muscle gene products. J Clin Invest 114:370-378

Adams J (2001). Proteasome inhibition in cancer: development of PS-341. Semin Oncol 28:613-619

Akerblom IE, Murry LK (1998). Human cachexia associated protein. U.S. Patent 5,583,192, issued to Incyte Pharmaceuticals, California

Argiles JM, Meijsing SH, Pallares-Trujillo J, Guirao X, Lopez-Soriano FJ (2001). Cancer cachexia: a therapeutic approach. Med Res Rev 21:83-101

Arlt A, Schafer H (2002). NFkappaB-dependent chemoresistance in solid tumors. Int J Clin Pharmacol Ther 40:336-347

Arsenieva D, Jeffery CJ, 2002. Conformational changes in phosphoglucose isomerase induced by ligand binding. J Mol Biol 323:77-84

Baumann M, Kappl A, Lang T, Brand K, Siegfried W, Paterok E (1990). The diagnostic validity of the serum tumor marker phosphohexose isomerase (PHI) in patients with gastrointestinal, kidney, and breast cancer. Cancer Invest 8:351-356

Bendre MS, Gaddy-Kurten D, Mon-Foote T, Akel NS, Skinner RA, Nicholas RW, Suva LJ (2002). Expression of interleukin 8 and not parathyroid hormone-related protein by human breast cancer cells correlates with bone metastasis in vivo. Cancer Res 62:5571-5579

Berenson JR, Ma HM, Vescio R (2001). The role of nuclear factor-kappaB in the biology and treatment of multiple myeloma. Semin Oncol 28:626-633

Black K, Garrett IR, Mundy GR (1991). Chinese hamster ovarian cells transfected with the murine interleukin-6 gene cause hypercalcemia as well as cachexia, leukocytosis and thrombocytosis in tumor-bearing nude mice. Endocrinol 128:2657-2659

Bodansky O (1954). Serum phosphohexose isomerase in cancer II: an index of tumor growth in metastatic carcinoma of the breast. Cancer 7:1200-1226

Cabal-Manzano R, Bhargava P, Torres-Duarte A, Marshall J, Bhargava P, Wainer IW (2001). Proteolysis-inducing factor is expressed in tumours of patients with gastrointestinal cancers and correlates with weight loss. Br J Cancer 84:1599-1601

Caffier H, Brandau H (1983). Serum tumor markers in metastatic breast cancer and course of disease. Cancer Detect Prev 6:451-457

Cahlin C, Korner A, Axelsson H, Wang W, Lundholm K, Svanberg E (2000). Experimental cancer cachexia: the role of host-derived cytokines interleukin (IL)-6, IL-12, interferon-gamma, and tumor necrosis factor alpha evaluated in gene knockout, tumor-bearing mice on C57 Bl background and eicosanoid-dependent cachexia. Cancer Res 60:5488-5493

Callander NS, Roodman GD (2001). Myeloma bone disease. Semin Hematol 38:276-285

Capparelli C, Kostenuik PJ, Morony S, Starnes C, Weimann B, Van G, Scully S, Qi M, Lacey DL, Dunstan CR (2000). Osteoprotegerin prevents and reverses hypercalcemia in a murine model of humoral hypercalcemia of malignancy. Cancer Res 60:783-787

Carbo N, Lopez-Soriano J, Costelli P, Busquets S, Alvarez B, Baccino FM, Quinn LS, Lopez-Soriano FJ, Argiles JM (2000). Interleukin-15 antagonizes muscle protein waste in tumour-bearing rats. Br J Cancer 83:526-531

Crown AL, Cottle K, Lightman SL, Falk S, Mohamed-Ali V, Armstrong L, Millar AB, Holly JM (2002). What is the role of the insulin-like growth factor system in the pathophysiology of cancer cachexia, and how is it regulated? Clin Endocrinol (Oxf) 56:723-733

Cher ML (2001). Mechanisms governing bone metastasis in prostate cancer. Curr Opin Urol 11:483-488

Chirgwin JM, Guise TA (2000). Molecular mechanisms of tumor-bone interactions in osteolytic metastases. Crit Rev Eukaryot Gene Expr 10:159-178

Colangeli R, Heijbel A, Williams AM, Manca C, Chan J, Lyashchenko K, Gennaro ML (1998). Three-step purification of lipopolysaccharide-free, polyhistidine-tagged recombinant antigens of Mycobacterium tuberculosis. J Chromatogr B Biomed Sci Appl 714:223-235

Coleman RE, Rubens RD (1987). The clinical course of bone metastases from breast cancer. Br J Cancer 55:61-66

Coulombe P, Rodier G, Pelletier S, Pellerin J, Meloche S (2003). Rapid turnover of extracellular signal-regulated kinase 3 by the ubiquitin-proteasome pathway defines a novel paradigm of mitogen-activated protein kinase regulation during cellular differentiation. Mol Cell Biol 23:4542-4558.

Crown AL, Cottle K, Lightman SL, Falk S, Mohamed-Ali V, Armstrong L, Millar AB, Holly JM (2002). What is the role of the insulin-like growth factor system in the pathophysiology of cancer cachexia, and how is it regulated? Clin Endocrinol 56:723-733

Davies C, Muirhead H, Chirgwin J (2003). The structure of human phosphoglucose isomerase complexed with a transition-state analogue. Acta Crystallogr D Biol Crystallogr 59:1111-1113

Dehoux M, Van Beneden R, Pasko N, Lause P, Verniers J, Underwood L, Ketelslegers JM, Thissen JP (2004). Role of the IGF-I decline in the induction of Atrogin-1/MAFbx during fasting and diabetes. Endocrinology Jul 29 [Epub ahead of print]

De La Mata J, Uy HL, Guise TA, Story B, Boyce BF, Mundy GR, Roodman GD (1995). Interleukin-6 enhances hypercalcemia and bone resorption mediated by parathyroid hormone-related protein in vivo. J Clin Invest 95: 2846-2852

Draghia-Akli R, Hahn KA, King GK, Cummings KK, Carpenter RH (2002). Effects of plasmid-mediated growth hormone-releasing hormone in severely debilitated dogs with cancer. Mol Ther 6:830-836

Endo K, Katsumata K, Iguchi H, Kubodera N, Teramoto T, Ikeda K, Fujita T, Ogata E (1998). Effect of combination treatment with a vitamin D analog (OCT) and a bisphosphonate (AHPrBP) in a nude mouse model of cancer-associated hypercalcemia. J Bone Miner Res 13:1378-1383

Esper PS, Pienta KJ (1997). Supportive care in the patient with hormone refractory prostate cancer. Semin Urol Oncol 15:56-64

Fearon K, Moses A (2002). Cancer cachexia. Int J Cardiol 85:73-81

Fernandez C, Sainz RD (1997). Pathways of protein degradation in L6 myotubes. Proc Soc Exp Biol Med 214:242-247

Foley PL, Lipuma JJ, Feldman SH (2004). Outbreak of otitis media caused by Burkholderia gladioli infection in immunocompromised mice. Comp Med 54:93-99

Giordano A, Calvani M, Petillo O, Carteni' M, Melone MR, Peluso G (2003). Skeletal muscle metabolism in physiology and in cancer disease. J Cell Biochem 90:170-186

Glass DJ (2003). Molecular mechanisms modulating muscle mass. Trends Mol Med 9:344-350

Gomes-Marcondes MC, Smith HJ, Cooper JC, Tisdale MJ (2002). Development of an in-vitro model system to investigate the mechanism of muscle protein catabolism induced by proteolysis-inducing factor. Br J Cancer 86:1628-1633

Guise TA, Chirgwin JM, Favarato G, Boyce BF, Mundy GR (1992). Chinese hamster ovarian cells transfected with human parathyroid hormone-related protein cDNA cause hypercalcemia in nude mice. Lab Invest 67:477-485

Guise TA, Yin JJ, Taylor SD, Kumagai Y, Dallas M, Boyce BF, Yoneda T, Mundy GR (1996). Evidence for a causal role of parathyroid hormone-related protein in the pathogenesis of human breast cancer-mediated osteolysis. J Clin Invest 98:1544-1549

Guise TA, Mundy GR (1998). Cancer and bone. Endocr Rev 19:18-54

Guttridge DC, Mayo MW, Madrid LV, Wang C-Y, Baldwin AS Jr (2000). NF-6B-induced loss of MyoD messenger RNA: Possible role in muscle decay and cachexia . Science 289: 2363-2366

von Haehling S, Genth-Zotz S, Anker S, Volk H (2002). Cachexia: a therapeutic approach beyond cytokine antagonism. Int J Cardiol 85:173-183

Hardman WE (2002). Omega-3 fatty acids to augment cancer therapy. J Nutr 132(11 Suppl):3508S-3512S

Hasselgren PO, Fischer JE (2001). Muscle cachexia: current concepts of intracellular mechanisms and molecular regulation. Ann Surg 233:9-17

Hasselgren PO, Wray C, Mammen J (2002). Molecular regulation of muscle cachexia: it may be more than the proteasome. Biochem Biophys Res Commun 290:1-10

Hideshima T, Chauhan D, Richardson P, Mitsiades C, Mitsiades N, Hayashi T, Munshi N, Dang L, Castro A, Palombella V, Adams J, Anderson KC (2002). NF-kappa B as a therapeutic target in multiple myeloma. J Biol Chem 277:16639-16647

Iguchi H, Onuma E, Sato K, Sato K, Ogata E (2001). Involvement of parathyroid hormone-related protein in experimental cachexia induced by a human lung cancer-derived cell line established from a bone metastasis specimen. Int J Cancer 94:24-27
Inui A (2002). Cancer anorexia-cachexia syndrome: current issues in research and management. CA Cancer J Clin 52:72-91

Jagoe RT, Goldberg AL (2001). What do we really know about the ubiquitin-proteasome pathway in muscle atrophy? Curr Opin Clin Nutr Metab Care 4:183-190

Jho DH, Babcock TA, Tevar R, Helton WS, Espat NJ (2002). Eicosapentaenoic acid supplementation reduces tumor volume and attenuates cachexia in a rat model of progressive non-metastasizing malignancy. JPEN J Parenter Enteral Nutr 26:291-297

Kalra P, Tigas S (2002). Regulation of lipolysis: natriuretic peptides and the development of cachexia. Int J Cardiol 85:125-132

Kotler DP (2000). Cachexia. Ann Intern Med 133:622-634

Lagana A, Duchaine T, Raz A, DesGroseillers L, Nabi IR (2000). Expression of autocrine motility factor/phosphohexose isomerase in Cos7 cells. Biochem Biophys Res Commun 273:213-218

Lange PH, Vessella RL (1998-9). Mechanisms, hypotheses and questions regarding prostate cancer micrometastases to bone. Cancer Metastasis Rev 17:331-336

Langen RC, Schols AM, Kelders MC, Wouters EF, Janssen-Heininger YM (2001). Inflammatory cytokines inhibit myogenic differentiation through activation of nuclear factor-kappaB. FASEB J 15:1169-1180

Lazarus DD, Destree AT, Mazzola LM, McCormack TA, Dick LR, Xu B, Huang JQ, Pierce JW, Read MA, Coggins MB, Solomon V, Goldberg AL, Brand SJ, Elliott PJ (1999). A new model of cancer cachexia: contribution of the ubiquitin-proteasome pathway. Am J Physiol 277:E332-E341

Lecker SH (2003). Ubiquitin-protein ligases in muscle wasting: multiple parallel pathways? Curr Opin Clin Nutr Metab Care 6:271-275

Lecker SH, Jagoe RT, Gilbert A, Gomes M, Baracos V, Bailey J, Price SR, Mitch WE, Goldberg AL (2004). Multiple types of skeletal muscle atrophy involve a common program of changes in gene expression. FASEB J 18:39-51

Lee SW, Dai G, Hu Z, Wang X, Du J, Mitch WE (2004). Regulation of muscle protein degradation: coordinated control of apoptotic and ubiquitin-proteasome systems by phosphatidylinositol 3 kinase. J Am Soc Nephrol 15:1537-1545.

Li X, Choi SJ, Roodman GD, Guise TA, Chirgwin JM (2000). Autocrine motility factor (AMF) stimulates periosteal new bone formation. Calcified Tissue Internat 66(Suppl 1):S56 (Abstract O-26)

Lorite MJ, Thompson MG, Drake JL, Carling G, Tisdale MJ (1998). Mechanism of muscle protein degradation induced by a cancer cachectic factor. Br J Cancer 78:850-856

Lorite MJ, Smith HJ, Arnold JA, Morris A, Thompson MG, Tisdale MJ (2001). Activation of ATP-ubiquitin-dependent proteolysis in skeletal muscle in vivo and murine myoblasts in vitro by a proteolysis-inducing factor (PIF). Br J Cancer 85:297-302

Matthys P, Dijkmans R, Proost P, Van Damme J, Heremans H, Sobis H, Billiau A (1991). Severe cachexia in mice inoculated with interferon-gamma-producing tumor cells. Int J Cancer 49:77-82

Matthys P, Billiau A (1997). Cytokines and cachexia. Nutrition 13:763-770

McDevitt H (2000). A new model for rheumatoid arthritis? Arthritis Res 2:85-89

McPherron AC, Lawler AM, Lee SJ (1997). Regulation of skeletal muscle mass in mice by a new TGF-beta superfamily member. Nature 387:83-90

Meazza R, Lollini PL, Nanni P, De Giovanni C, Gaggero A, Comes A, Cilli M, Di Carlo E, Ferrini S, Musiani P (2000). Gene transfer of a secretable form of IL-15 in murine

adenocarcinoma cells: effects on tumorigenicity, metastatic potential and immune response. Int J Cancer 87:574-581

Mitch WE, Price SR (2001). Transcription factors and muscle cachexia: is there a therapeutic target? Lancet 357:734-735

Mundy G (2001). Preclinical models of bone metastases. Semin Oncol 28(Suppl 11):2-8

Mundy GR (2002). Metastasis to bone: causes, consequences and therapeutic opportunities. Nat Rev Cancer 2:584-593

Nagy T, Janossy T, Vizler C, Bohus K, Joo F, Vegh P, Duda E (1999). Pathophysiological effects of human TNF-alpha-producing tumor xenografts in immunosuppressed mice. APMIS 107:903-912

Nelson KA (2000). Modern management of the cancer anorexia-cachexia syndrome. Curr Oncol Rep 2:362-368

Norton JA, Moley JF, Green MV, Carson RE, Morrison SD (1985). Parabiotic transfer of cancer anorexia/cachexia in male rats. Cancer Res 45:5547-5552

Ogata E (2000). Parathyroid hormone-related protein as a potential target of therapy for cancer-associated morbidity. Cancer 88(S12):2909-2911

Ozaki Y, Oyama T, Kume S (1989). Exacerbation of toxic effects by endotoxin contamination of recombinant human tumor necrosis factor. Cancer Chemother Pharmacol 23:231-237

Parma M, Diament M, Garcia C, Piccinni E, Mondelo N, Klein S (1999). Mechanisms of paraneoplastic syndromes in mice bearing a spontaneous lung adenocarcinoma. Tumour Biol 20:304-311

Quinn LS, Anderson BG, Drivdahl RH, Alvarez B, Argiles JM (2002). Overexpression of interleukin-15 induces skeletal muscle hypertrophy in vitro: implications for treatment of muscle wasting disorders. Exp Cell Res 280:55-63

Read J, Pearce J, Li X, Muirhead H, Chirgwin J, Davies C (2001). The crystal structure of human phosphoglucose isomerase at 1.6 A resolution: implications for catalytic mechanism, cytokine activity and haemolytic anaemia. J Mol Biol 309:447-463

Reinheckel T, Grune T, Davies KJ (2000). The measurement of protein degradation in response to oxidative stress. Methods Mol Biol 99:49-60..

Roth SM, Walsh S (2004). Myostatin: a therapeutic target for skeletal muscle wasting. Curr Opin Clin Nutr Metab Care 7:259-263

Roubenoff R, Roubenoff RA, Ward LM, Holland SM, Hellmann DB (1992). Rheumatoid cachexia: depletion of lean body mass in rheumatoid arthritis. Possible association with tumor necrosis factor. J Rheumatol 19:1505-1510

Ross JA, Fearon KC (2002). Eicosanoid-dependent cancer cachexia and wasting. Curr Opin Clin Nutr Metab Care 5:241-248

Sacheck JM, Ohtsuka A, McLary SC, Goldberg AL (2004). IGF-1 stimulates muscle growth by suppressing protein breakdown and expression of atrophy-related ubiquitin-ligases, atrogin-1 and MuRF1. Am J Physiol Endocrinol Metab Apr 20 [Epub ahead of print]

Sandri M, Sandri C, Gilbert A, Skurk C, Calabria E, Picard A, Walsh K, Schiaffino S, Lecker SH, Goldberg AL (2004). Foxo transcription factors induce the atrophy-related ubiquitin ligase atrogin-1 and cause skeletal muscle atrophy. Cell 117:399-412

Schwartz MW, Morton GJ (2002). Keeping hunger at bay. Nature 418:595-597

Spate U, Schulze PC (2004). Proinflammatory cytokines and skeletal muscle. Curr Opin Clin Nutr Metab Care 7:265-269

Stitt TN, Drujan D, Clarke BA, Panaro F, Timofeyva Y, Kline WO, Gonzalez M, Yancopoulos GD, Glass DJ (2004). The IGF-1/PI3K/Akt pathway prevents expression of muscle atrophy-induced ubiquitin ligases by inhibiting FOXO transcription factors. Mol Cell 14:395-403

Taylor WE, Bhasin S, Artaza J, Byhower F, Azam M, Willard DH Jr, Kull FC Jr, Gonzalez-Cadavid N (2001). Myostatin inhibits cell proliferation and protein synthesis in C2C12 muscle cells. Am J Physiol Endocrinol Metab 280:E221-228

Thompson MG, Palmer RM, Thom A, Mackie SC, Morrison KS, Harris CI (1996). Measurement of protein degradation by release of labelled 3-methylhistidine from skeletal muscle and non-muscle cells. J Cell Physiol 166:506-511

Tilignac T, Temparis S, Combaret L, Taillandier D, Pouch MN, Cervek M, Cardenas DM, Le Bricon T, Debiton E, Samuels SE, Madelmont JC, Attaix D (2002). Chemotherapy inhibits skeletal muscle ubiquitin-proteasome-dependent proteolysis. Cancer Res 62:2771-2777

Tisdale MJ (1998). New cachexic factors. Curr Opin Clin Nutr Metab Care 1:253-256

Tisdale MJ (2000). Metabolic abnormalities in cachexia and anorexia. Nutrition 16:1013-1014

Tisdale MJ (2001). Loss of skeletal muscle in cancer: biochemical mechanisms. Front Biosci. 6:D164-174

Tisdale MJ (2002). Cachexia in cancer patients. Nat Rev Cancer 2:862-871

Tisdale MJ (2002a). Biochemical mechanisms of cellular catabolism. Curr Opin Clin Nutr Metab Care 5:401-405

Tisdale MJ (2003). Pathogenesis of cancer cachexia. J Support Oncol 1:159-168

Todorov PT, Deacon M, Tisdale MJ (1997). Structural analysis of a tumor-produced sulfated glycoprotein capable of initiating muscle protein degradation. J Biol Chem 272:12279-12288

Tohgo A, Kumazawa E, Akahane K, Asakawa A, Inui A (2002). Anticancer drugs that induce cancer-associated cachectic syndromes. Expert Rev Anticancer Ther 2:121-129

Tsutsumi S, Hogan V, Nabi IR, Raz A (2003). Overexpression of the autocrine motility factor/phosphoglucose isomerase induces transformation and survival of NIH-3T3 fibroblasts. Cancer Res 63:242-249.

Valorie AM (2000). Thalidomide. A new beginning. Cancer Pract 8:101-103

Watchorn TM, Waddell I, Dowidar N, Ross JA (2001). Proteolysis-inducing factor regulates hepatic gene expression via the transcription factors NF-(kappa)B and STAT3. FASEB J 15:562-564

Watchorn TM, Waddell I, Ross JA (2002). Proteolysis-inducing factor differentially influences transcriptional regulation in endothelial subtypes. Am J Physiol Endocrinol Metab 282:E763-769

Whitehouse AS, Smith HJ, Drake JL, Tisdale MJ (2001). Mechanism of attenuation of skeletal muscle protein catabolism in cancer cachexia by eicosapentaenoic acid. Cancer Res 61:3604-3609

Yamaguchi A (1995). Regulation of differentiation pathway of skeletal mesenchymal cells in cell lines by transforming growth factor-beta superfamily. Semin Cell Biol 6:165-173.

Yates AJ, Boyce BF, Favarato G, Aufdemorte TB, Marcelli C, Kester MB, Walker R, Langton BC, Bonewald LF, Mundy GR (1992). Expression of human transforming growth factor alpha by Chinese hamster ovarian tumors in nude mice causes hypercalcemia and increased osteoclastic bone resorption. J Bone Miner Res 7:847-853

Yin JJ, Selander K, Chirgwin JM, Dallas M, Grubbs BG, Wieser R, Massagué J, Mundy GR, Guise TA (1999). TGF-$ signaling blockade inhibits PTHrP secretion by breast cancer cells and bone metastases development. J Clin Invest 103:197-206

Yoneda T, Alsina MA, Chavez JB, Bonewald L, Nishimura R, Mundy GR (1991a). Evidence that tumor necrosis factor plays a pathogenetic role in the paraneoplastic syndromes of cachexia, hypercalcemia, and leukocytosis in a human tumor in nude mice. J Clin Invest 87:977-985

Yoneda T, Alsina MM, Watatani K, Bellot F, Schlessinger J, Mundy GR (1991b). Dependence of a human squamous carcinoma and associated paraneoplastic syndromes on the epidermal growth factor receptor pathway in nude mice. Cancer Res 51:2438-2443

You J, Wang M, Aoki T, Tamura TA, Pickart CM (2003). Proteolytic targeting of transcriptional regulator TIP120B by a HECT domain E3 ligase. J Biol Chem 278:23369-23675.

Zhou S, Kestell P, Tingle MD, Paxton JW (2002). Thalidomide in cancer treatment: a potential role in the elderly? Drugs Aging 19:85-100

Zimmers TA, Davies MV, Koniaris LG, Haynes P, Esquela AF, Tomkinson KN, McPherron AC, Wolfman NM, Lee SJ (2002). Induction of cachexia in mice by systemically administered myostatin. Science 296:1486-1488

FIGURES and LEGENDS

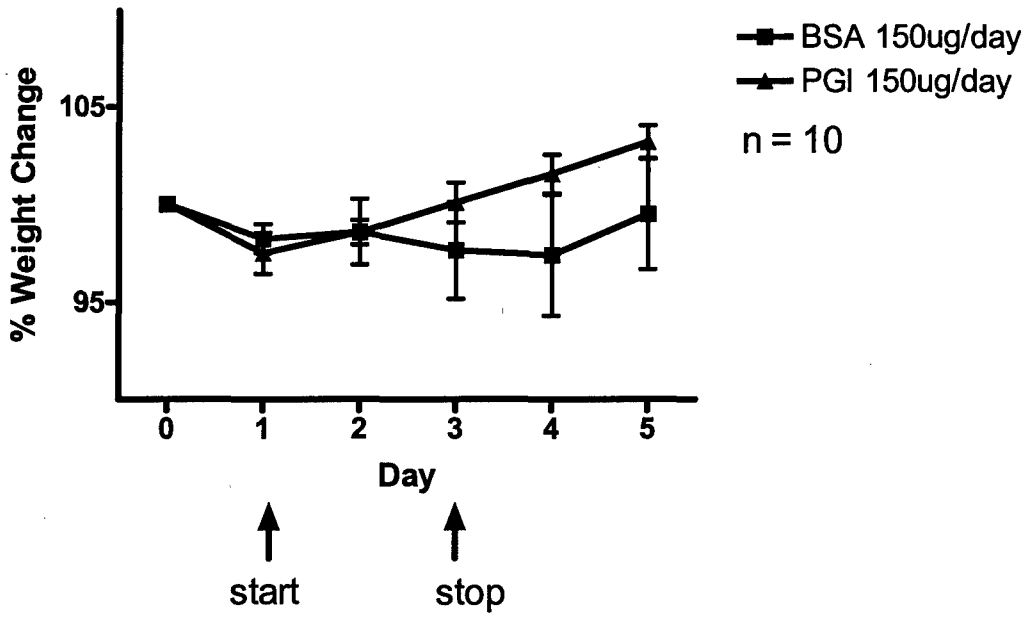

Figure 1. In the experimental protocol, Balb/C nu/nu mice, approximately 25g in weight, were given the factor as sterile intraperitoneal (i.p.) injections of protein in PBS at 8 AM, noon, and 4 PM. Blood levels of PGI/AMF were measured at the 4 PM time. Animals were weighed at the same time. Animals were injected on days 1, 2, and 3 and allowed to recover for two more days. Injections were of 150 μg purified mouse AMF/PGI or BSA (Sigma) in 100 μl of sterile PBS. The curves are not statistically significant ($p > 0.05$) between the two groups by 2-way ANOVA, with n = 10 mice/group.

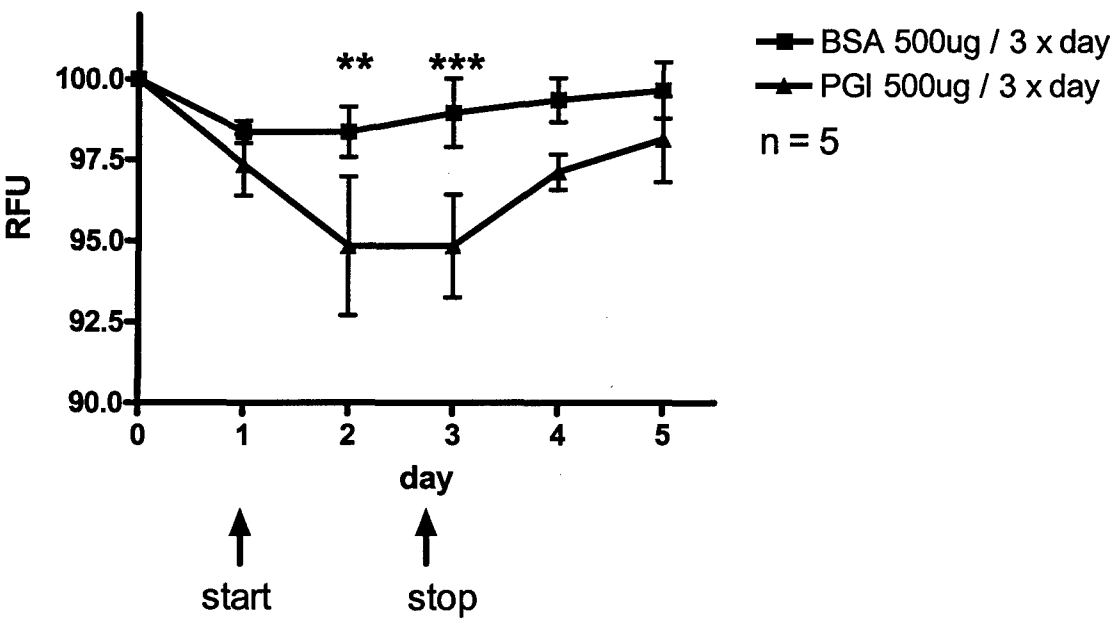

Figure 2. Protocol was similar to that described under Figure 1, except that the injections were of 500 μg aliquots of the proteins, in the same volume of PBS as before. There were n = 5 mice per group. The curves were analyzed for statistical significance by 2-way ANOVA, and $p < 0.0001$. Significance of differences between the two curves at each time point were calculated by comparing replicates of the means by row with Bonferroni's post-test using the statistics programs in GraphPad Prizm. ** $p < 0.01$; *** $p < 0.001$. Other points n.s. ($p > 0.05$).

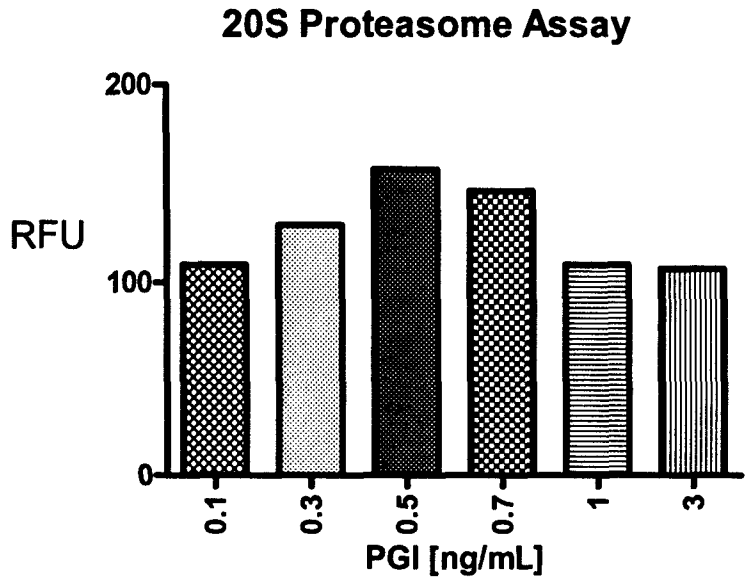

Figure 3. C2C12 mouse myoblasts (ATCC) were grown to confluence, changed to serum-free medium for 24 hrs, and then treated for 24 hrs with the indicated concentrations of recombinant mouse PGI/AMF. These cells are routinely studied for the induction of proteasomal activity (Coulombe et al, 2003: You et al, 2003), as well as being used for models of skeletal muscle cell function and differentiation (Yamaguchi, 1995). Cells were harvested, lysed by three cycles of freeze/thawing, homogenized, and centrifuged for 10 minutes at 14,000xg and 4°C to sediment debris. The supernatants were adjusted to a constant protein concentration of 50 μg/ml and assayed for 20S proteasomal chymotryptic activity (Reinheckel et al, 2000) with the fluorogenic substrate, succinyl-LLVY-AMC (Calbiochem) for 1 hr at 37°C. Control values not shown, since these continue to be highly variable, and we have not yet succeeded in establishing a reproducible negative control for the assay. Differentiation of the myoblasts into myotubes, by culturing in the presence of horse serum, may resolve this problem (experiments underway).

J Musculoskel Neuron Interact 2004; 4(3):308-318

Review Article

Tumor-bone cellular interactions in skeletal metastases

J.M. Chirgwin, K.S. Mohammad, T.A. Guise

Division of Endocrinology, Department of Medicine, University of Virginia, Charlottesville, USA

Abstract

Human tumor cells inoculated into the arterial circulation of immunocompromised mice can reliably cause bone metastases, reproducing many of the clinical features seen in patients. Animal models permit the identification of tumor-produced factors, which act on bone cells, and of bone-derived factors. Local interactions stimulated by these factors drive a vicious cycle between tumor and bone that perpetuates skeletal metastases. Bone metastases can be osteolytic, osteoblastic, or mixed. Parathyroid hormone-related protein, PTHrP, is a common osteolytic factor, while vascular endothelial growth factor and interleukins 8 and 11 also contribute. Osteoblastic metastases can be caused by tumor-secreted endothelin-1, ET-1. Other potential osteoblastic factors include bone morphogenetic proteins, platelet-derived growth factor, connective tissue growth factor, stanniocalcin, N-terminal fragments of PTHrP, and adrenomedullin. Osteoblasts are the main regulators of osteoclasts, and stimulation of osteoblast proliferation can increase osteoclast formation and activity. Thus, combined expression of osteoblastic and osteolytic factors can lead to mixed metastases or to increased osteolysis. Prostate-specific antigen is a protease, which can cleave PTHrP and thus change the balance of osteolytic versus osteoblastic responses to metastatic tumor cells. Bone itself stimulates tumor by releasing insulin-like growth factors and transforming growth factor-β. Secreted factors transmit the interactions between tumor and bone. They provide novel targets for therapeutic interactions to break the vicious cycle of bone metastases. Clinically approved bisphosphonate anti-resorptive drugs reduce the release of active factors stored in bone, and PTHrP-neutralizing antibody, inhibitors of the RANK ligand pathway, and ET-1 receptor antagonist are in clinical trials. These adjuvant therapies act on bone cells, rather than the tumor cells. Recent gene array experiments identify additional factors, which may in the future prove to be clinically important targets.

Keywords: Cancer, Breast, Prostate, Bone Metastasis, Parathyroid Hormone-Related, Protein, Endothelin, Adrenomedullin, Transforming Growth Factor-β, Prostate-Specific Antigen

Introduction

The majority of patients dying from cancer of the breast or prostate have metastases to the skeleton. The affinity of these and several other solid tumors for this metastatic site is the consequence of the special microenvironment provided by bone. Stephen Paget in 1889 proposed the seed and soil hypothesis: bone provides the fertile soil in which certain cancer cell seeds prefer to grow. We now appreciate that mineralized bone matrix is a rich storehouse of growth factors[1], which are mobilized by osteoclastic bone resorption. The released growth factors enrich the local microenvironment. A main effect of the factors appears to be alteration of the tumor cell phenotype rather than an increased growth rate. Tumor cells in turn secrete additional factors that act upon bone cells, causing the responses that characterize the osteolytic and osteoblastic metastases. Local interactions between tumor cells and bone form a vicious cycle, which underlies the development of skeletal metastases[2,3]. Interactions between tumor cells and bone cells change the phenotypes of both.

The basic mechanisms of cancer metastases to specific sites have been controversial. Cancer cells *in vivo* continue to mutate. The ability of cancer cells to metastasize is characteristic of advanced disease and could occur only after the gradual accumulation of a necessary set of pro-metastatic mutations[4]. However, recent experiments suggest that a constellation of expressed genes necessary for metastasis to bone pre-exists within the primary breast tumor[5]. Thus, bone-specific metastases are the consequence of a selection

The authors have no conflict of interest.

Corresponding author: John M. Chirgwin, Ph.D. Division of Endocrinology, PO Box 801421, Department of Medicine, University of Virginia, Charlottesville, VA 22908, USA
E-mail: jc3qb@virginia.edu

Accepted 11 February 2004

of variants from a heterogeneous population of cells within the primary tumor, plus changes in gene expression induced by bone factors[6]. Cells of the osteoblastic lineage appear to be the main targets of tumor-secreted factors. Bone-derived transforming growth factor-β (TGFβ) is a major factor regulator of tumor cell behavior in bone.

There are no convenient animal models where primary tumors reproducibly metastasize to bone. Many of the results described here use an animal model in which human tumor cells are inoculated into immuno-deficient mice. Injection into the venous circulation most often results in tumor cell entrapment within the capillary beds of the lung or liver. However, careful tumor administration directly into the left cardiac ventricle can result in 100% incidence of bone metastases with many tumor cell lines (Table 1). Osteolytic lesions are detected by X-ray as early as 3 weeks and can be quantified by image analysis. Osteoblastic lesions may take up to 6 months to develop in nude mice, and the lesions cannot be quantified radiographically.

Osteolytic metastases

Destructive bone lesions are characteristic of breast cancer. The most prominent cause of bone destruction is parathyroid hormone-related protein, PTHrP, which is secreted by many cancer types and, when systemically elevated, is responsible for humoral hypercalcemia of malignancy (HHM)[7]. Breast and lung cancer cells that secrete PTHrP in concentrations insufficient to induce HHM still cause extensive osteolytic bone destruction in nude mice. Bone lesions and tumor burden can be significantly decreased, and survival increased, by treatment with PTHrP-neutralizing antibody[8,9]. The antibody has been humanized and is in clinical trials against HHM.

PTHrP was originally suspected to play a role in osteolytic metastases based on its known role as a stimulator of hypercalcemia[7], plus its high expression by tumor cells in bone versus soft tissue sites in patients[10,11]. These results suggested that PTHrP expression by the primary tumor might be prognostic of metastases to bone. This is not the case. In a prospective study, PTHrP expression by the primary tumor was an independent prognostic marker of improved survival and *decreased* metastasis to bone[12]. PTHrP is a complex, multifunctional protein and appears to play independent roles in primary and metastatic cells. It is likely that the expression of PTHrP by breast cancer cells in bone is the result of induction of its gene by factors in bone, such as TGFβ[13].

PTHrP cannot be the only factor responsible for bone metastases, and a number of other proteins play either contributory or PTHrP-independent roles[2]. Candidate factors that may contribute to PTHrP-induced osteolytic lesions are interleukin (IL)-11, macrophage colony-stimulating factor (M-CSF), and vascular endothelial growth factor (VEGF)[14]. PTHrP-independent factors have also been reported, including IL-8, which can directly stimulate the osteoclast[15,16].

Kang et al. compared less- and more-metastatic variants of a breast cancer cell line by gene expression profiling[5]. They identified mRNAs whose expression strongly correlated with increased bone metastasis. Five of the mRNAs encoded IL-11, matrix metalloproteinase (MMP)-1 osteopontin, connective tissue growth factor (CTGF), and CXCR-4. MMP-1 is an interstitial collagenase made by osteoblasts. It cleaves collagen at a site resistant to osteoclastic enzyme hydrolysis and may be rate-limiting in normal bone resorption[17]. Osteopontin plays a complex role in metastasis, including modulation of anti-tumor immune responses[18] and is differentially regulated in tumor cells metastatic to bone versus other sites[19]. CTGF is a potent osteoblast-stimulatory factor[20], as well as being expressed by tumor cells. CXCR-4 is the receptor for the chemokine SDF-1 and functions in the attraction of breast cancer cells to specific metastatic sites including, but not limited to, bone[21]. Kang et al.[5] found that the pro-metastatic gene set was coordinately increased in cells that pre-existed in the original cell population. The authors attempted to convert low-metastatic MDA-MB-231 breast cancer cell line clones into ones highly metastatic to bone by overexpressing each of the five individual factors. They found that conversion of the cells to a phenotype of aggressive metastasis to bone required co-transduction of combinations of four of the five factors. The results strongly support a multi-factorial mechanism underlying organ-specific metastases.

Many osteolytic factors act via osteoblasts and stimulate osteoclastic bone resorption indirectly, rather than acting directly on cells of the osteoclast lineage[22]. This has been shown for PTHrP, which induces osteoblastic expression of RANK ligand[23]. IL-11 can act similarly, while M-CSF and VEGF serve as co-factors for the RANK ligand-stimulated differentiation of hemopoietic precursors into active osteoclasts.

Osteoblastic metastases

Metastases with net formation of disorganized new bone are characteristic of prostate cancer[24] and also occur in 15% of breast cancer bone metastases. The tumor-induced lesions are characterized by formation of new but abnormal and disorganized new bone, and they are accompanied by increased bone resorption. A number of candidate factors made by tumor cells could stimulate osteoblasts, but progress has lagged in the area until recently. Endothelin-1 (ET-1), a 21-amino acid vasoactive peptide, is a potent stimulator of new bone formation. It is secreted by tumor cells[25] and can cause osteoblastic metastases in the nude mouse model. Metastases are effectively blocked with a selective antagonist of the endothelin A receptor[26,27]. This orally active antagonist is in clinical trials in men with advanced metastatic prostate cancer[28-30]. The vicious cycle model predicts that osteoblasts, osteoclasts and tumor cells cooperate to cause the pathology of bone metastases. The endothelin receptor antagonist blocks the activation of osteoblasts by tumor-produced ET-1. It also decreases osteoclastic bone resorption, as indicated by decreases in markers of resorp-

Cell Line	Bone Metastases	PTHrP	IL-6[F]	IL-11[F]	VEGF	Other Osteolytic Factors	ET-1	AM	Other Blastic Factors
Breast									
ZR-75-1	OB	0	0	0	99±1.5		81±5		
MCF-7	OB	0	3.3±0.2	0	180±2		19±2	+[A]	PDGF[B]
					[171±20][M]				
T47D	OB	0			[68±12][M]		227±12	+[A]	
BT483	M	0					22±6		
MDA-	OL	0.54±0.1	360	240±3	1258±34	IL-8[C]	0	+	CTGF[D]
MB-231					[1021±23][M]				
BT549	OL	0.44±0.12					0		
MDA-	OL	0.29±0.12			[91±7][M]		0		
MB-435s									
HS578T	N	0.46±0.05					3±2		
MDA-	N	0.4±0.4					0		
MB-436									
MDA-	N	0					0		
MB-361									
Prostate									
DU-145	N	0.75±0.08					23±2x	78±10[K]	
							[4±0.3][J]		
LNCaP	N	0.08±0.08			470[L]		0	0[K]	
							[1.2±0.2][J]		
PC-3	OL	12±0.8			<25[L]		0	+[E]	
							[5±0.3][J]	71±9[K]	
Lung									
RWGT2F	OL	64±2	117±2	0	1233±14				
SBC-5G	OL	+							
A549	OL	+[H]					+	+	
HARAI	OL	+							
Ovary									
CHO-K1	OL	+							

Table 1. Cancer Cell Lines and Phenotypes of Bone Metastases. PTHrP in pM/10^5 cells/48 hr by Nichols Institute 2-site IRMA. ET-1, IL-6, IL-11, VEGF in pg/ml/10^5 cells/48 hr by R&D Systems immunoassays. OB = osteoblastic, OL = osteolytic, M = mixed, N = none, when cells are inoculated into the arterial circulation of nude mice via the left cardiac ventricle. Most data from Yin et al.[27]. [A]AM = adrenomedullin (Miller et al.)[40]. [B]PDGF = platelet-derived growth factor B chain (Yi et al.)[97] [C]IL-8 = interleukin-8 (Bendre et al.)[15]; [D]CTGF = connective tissue growth factor (Kang et al.)[5]; [E]AM = adrenomedullin (Abasolo et al.)[43]; [F](Gallwitz et al.)[81]; [G](Miki et al.)[92]; [H](Hastings et al.)[42]; [I](Iguchi et al.)[9]; J(Chiao et al.)[93]; [K]Fmol/mg protein (Rocchi et al.)[41]; [L]pg/mg protein (Dall'Era et al.)[94]; [M]Arbitrary mRNA units (Scott et al.)[95]. Remaining data, indicated by pluses, are unpublished from the authors' laboratory. Note that some of these cells (MCF-7 and MDA-MB-231, for examples, vary in PTHrP production depending on source of the cell line). A number of cell lines, scored N here, cause bone responses when injected directly into the marrow cavity of the tibia or femur[96]. Most of the cell lines are of human origin.

tion seen in the patient trials. Conversely, bisphosphonates effectively reduce skeletal-related events in prostate cancer[31]. These observations support an important role for the vicious cycle in patients.

Other factors responsible for osteoblastic metastases remain to be identified. Such factors need to meet two initial criteria: 1) ability to stimulate osteoblastic new bone formation, and 2) expression by cancer cells. The bone morphogenetic proteins (BMPs) are obvious candidates, but a causal role in bone metastases has not been demonstrated. CTGF, identified in the experiments of Kang et al.[5] is another factor that stimulates osteoblasts[20,30]. It is a normal product of hypertrophic chondrocytes and is the second of three closely related gene products CCN1-3, which are selectively expressed in certain tumor types[33]. It is possible that CCN1 and CCN3 may contribute to bone metastases. CCN3 is expressed by prostate cancers[34], while CCN1, cyr61, is expressed by breast[35] and other cancers.

Adrenomedullin (AM) is a 52-amino acid vasoactive peptide with potent bone-stimulatory actions *in vitro*[36,37] and *in vivo*[38,91]. It is made by many cancers[39], including breast[40] and prostate[41]. We have recent data that it increases bone metastases *in vivo*. We tested the A549 human lung adenocarcinoma cell for its ability to form bone metastases when inoculated into the left cardiac ventricle. Animals developed osteolytic metastases after five weeks. These cells express PTHrP[42], ET-1, and AM. AM secretion was reduced 50% by stable expression of AM siRNA. These cells, made by Dr Alfredo Martinez at the National Cancer Institute, caused fewer metastases and increased survival, compared to empty vector-transfected A549 cells (unpublished results). In experiments the human prostate cancer cell line PC-3 was transfected with an AM expression DNA, resulting in a greater than ten-fold increase in AM secretion. These cells showed slower growth *in vitro* and as subcutaneous tumors[43]; this response is opposite to that found with many other tumors, where AM is an autocrine growth stimulatory and pro-angiogenic factor[39]. However, when these same PC-3 subclones were inoculated into nude mice, animal survival was less than half that of mice receiving control PC-3 cells. Mice with AM-overexpressing tumors showed accelerated osteolytic lesions and also adjacent areas of osteoblastic new bone formation (unpublished).

Another factor that could play a role in osteoblastic metastases is stanniocalcin, a polypeptide that is produced by cancer cells[44,45] and can stimulate new bone formation[46,47].

Mixed osteolytic/osteoblastic metastases

Mixed lesions are characteristic of both breast and prostate cancers. The effect of combined expression of osteolytic and osteoblastic factors on bone has not been studied, so the net response of bone at the metastatic site is unpredictable. As noted above, osteolytic factors such as PTHrP and IL-11 act on osteoblasts to increase expression of RANK ligand. We tested the effects of introducing the osteoblastic factor, ET-1, into the PTHrP-secreting MDA-MB-231 breast cancer cell line. Instead of converting the bone response from osteolytic to osteoblastic, the bone-destructive effects were enhanced by ET-1. Some of this effect may be caused by autocrine responses of the tumor cells to ET-1. We believe that osteoblastic factors can stimulate osteoblast proliferation, increasing the population of early osteoblasts[48]. The enlarged pool of early osteoblasts responds to osteolytic factors by increased expression of RANK ligand[49]. A similar mechanism may be involved in the metastases caused by A549 and PC-3 cells, described in the preceding paragraph. Both cell lines secrete PTHrP and adrenomedullin, and A549s make ET-1 as well (unpublished). Thus, expression of an osteoblastic factor may not simply convert an osteolytic tumor cell line into one that causes osteoblastic metastases.

Another puzzling question has been the role of PTHrP in osteoblastic metastases, especially those due to prostate cancers, which nearly always express PTHrP. A partial explanation was provided by the observation that prostate-specific antigen (PSA) is a serine protease, which cleaves PTHrP after phenylalanine residues 22 and 23[50,51]. The resulting fragment fails to activate the classical PTH/PTHrP receptor. This is not the end of the story. It was later observed that the inactive fragment PTHrP1-16 increased contraction of cardiac myocytes apparently by binding to the endothelin A receptor. Binding was attributed to a 4 amino acid near-identity between the two peptides[52]. We have extended these observations to bone. PTHrP1-23 is a potent stimulator of calvarial new bone formation at concentrations as low as 1nM (unpublished results), although this polypeptide has no detectable affinity for the type 1 PTH receptor. New bone formation was blocked by the endothelin A receptor antagonist, ABT-627. The results suggest that PSA proteolysis of PTHrP, rather than inactivating it, converts the protein from an osteolytic factor to a potent osteoblastic one. These preliminary results are *in vitro* and require confirmation of their physiological significance *in vivo*. PTHrP can also be cleaved by the neutral endopeptidases, neprilysin, which is expressed on the surface of prostate and bone cells[53]; so N-terminal fragments of PTHrP could play a role in normal bone metabolism.

Actions of bone on tumor cells

The effects of bone-derived factors on tumor cells remain understudied. Van der Pluijm et al. elegantly demonstrated that several mRNAs are increased in bone versus non-bone sites of human breast cancer metastases in nude mice[14]. RNA abundances were determined by species-specific RT-PCR. PTHrP, VEGFs and M-CSF were increased specifically in bone, while several mouse markers of host angiogenesis were similarly increased. These experiments did not identify the factor(s) responsible for the bone-specific mRNA induction. Hauschka et al.[1] found that insulin-like growth factors (IGFs) -2, then -1, were the most abundant factors in bone matrix, followed by TGFβ, after which were lower concentrations of

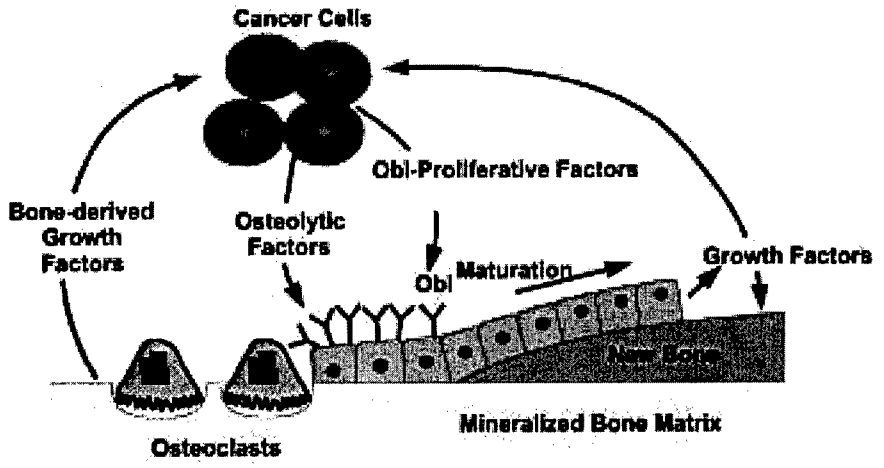

Figure 1. Tumor stimulation of osteoblasts can increase both new bone formation and resorption. Tumor products, such as endothelin-1 and adrenomedullin, stimulate osteoblast (Obl) proliferation. Immature osteoblasts respond to osteolytic cytokines, such as parathyroid hormone and interleukin-11, by expressing RANK ligand (Y). RANK ligand stimulates bone resorption by osteoclasts, which releases growth factors, such as transforming growth factor-β, from mineralized matrix. Mature osteoblasts synthesize growth factors, which are incorporated into bone and also enrich the local microenvironment. Growth factors stimulate tumor cells. Osteoblasts lose RANK ligand expression during maturation. The balance of osteoblast proliferation versus maturation, plus tumor production of factors like PTHrP, determines whether bone metastases are osteoblastic, osteolytic, or mixed. The new bone synthesized in osteoblastic metastases is disorganized and of poor mechanical quantity.

BMPs, fibroblast growth factors -1 and -2, and platelet-derived growth factor[1]. Of these, only TGFβ has been shown to play a direct role in stimulating tumor cells. TGFβ is growth-inhibitory in the early stages of tumorigenesis. Advanced cancers lose growth inhibition but retain TGFβ regulation of metastasis-promoting genes[54], such as CTGF and IL-11, identified by Kang et al.[5], and PTHrP[13,55]. In the MDA-MB-231 model of breast cancer metastasis to bone, detailed experiments showed that tumor cell expression of PTHrP is the major target of TGFβ and that TGFβ is the most important regulator of PTHrP[56]. These experiments also showed that dual pathways in the tumor cells, through p38 MAP kinase and through the Smad proteins, transmit TGFβ signaling to the nucleus. Osteoclastic bone resorption specifically activates TGFβ from its stored form in bone matrix[57]. This step may be another point at which the efficacy of bisphosphonates against bone metastases is exerted[31].

It is likely that in patients, tumor cells secrete sets of multiple proteins with actions on bone cells[5], and these sets may vary between metastatic sites within individuals. The list of the factors contributing to bone metastases is already large (Table 1) and will continue to grow. The effects of multiple factors and their relative expression levels probably change during the course of growth of a metastatic lesion, and the responses of the host cells at the metastatic site will also change over time. Many of the factors isolated from bone matrix[1] have been generically named as growth factors. However, tumor cell proliferation is generally growth factor-independent, and such proliferation is not rate-limiting for the progress of bone metastases. Experiments with inhibitors of bone responses to tumor cells (but which do not directly target the tumor cells) effectively decrease tumor burden[8,27,58,59]. These results suggest that paracrine interactions between tumor cells and bone cells are central regulators of skeletal metastases, and that the regulation is not via control of cell proliferation.

The vicious cycle

Animal models have established that bone metastases involve a vicious cycle between tumor cells and the skeleton (Figure 1). The cycle is driven by four obvious contributors: the tumor cells, bone-forming osteoblasts, bone-destroying osteoclasts, and organic bone matrix. Osteoclast formation and activity is controlled by the osteoblast, adding complexity to the vicious cycle. The mineralized matrix of bone provides a rich store of growth factors, such as insulin-like and transforming growth factors[1]. These factors are synthesized by osteoblasts and released by osteoclasts. The factors reach high local concentrations in the bone microenvironment and can act on tumor cells to encourage metastatic growth. The products released from resorbing bone attract tumor cells[60].

In turn, breast cancers secrete many factors that act on bone cells. It is likely that at sites of osteoblastic metastases, the tumor cells continue to secrete osteolytic factors, such as parathyroid hormone-related protein, which stimulate bone resorption. Therapies targeting the vicious cycle can decrease metastases by lowering the concentrations of growth factors in bone. It is characteristic of skeletal metastases that the properties of the bone are altered, contributing to the clinical pathology seen in patients. As disease progresses, the bone and the bone cells probably become more and more abnormal, under the continuing influence of tumor-secreted factors. It should be borne in mind that the images of metastases seen in animal models represent a much-simplified version of the clinical picture. The animal models are of much shorter duration and involve homogeneous tumor lines, whereas bone metastases in patients are much more heterogeneous, even within individual patients[61].

Roles of other cells in bone to skeletal metastases

It is an oversimplification to consider only osteoblasts and osteoclasts as the interacting partners of tumor cells in the vicious cycle of cancer bone metastases. Vascular endothelial cells are a major fourth cellular component. Most of the tumor-produced factors discussed above are vasoactive and many are pro-angiogenic, including endothelin[62], adrenomedullin[63], IL-8[64], the CCN proteins[33,65], stanniocalcin[66], as well as VEGF. PTHrP may be anti-angiogenic[67]. These same angiogenic factors are also increased by the hypoxic response in tumor cells, including endothelin[68], adrenomedullin[69], the CCN proteins[70,71], and stanniocalcin[72]. To further complicate the situation, many of these factors are both regulated by and regulators of VEGF, and many are also TGFβ-regulated genes. Thus, there must be an extremely complex cross-talk between endothelial cells, bone cells, and tumor cells at the metastatic site. Making sense of these interactions will require the development of novel and subtle experimental strategies.

Endothelial cells in bone differ from the cells lining blood vessels in other organs, which could contribute to the bone-tropism of certain tumors[73]. Just as tumor-secreted factors can alter the phenotypes of bone cells in the vicinity of metastases, such factors will probably also alter the behavior of endothelial cells. Van der Pluijm et al. observed specific changes in host vascular markers in bone versus non-bone metastatic sites[14]. Di Raimondo et al. similarly detected angiogenic factors at higher concentrations in bone marrow plasma than in the peripheral circulation of patients with multiple myeloma[74], suggesting the specific induction of angiogenic factor expression within the bone microenvironment of patients with cancer in the skeleton. Tumor cells are also likely to perturb the lineages of cells in bone. Bone marrow is a major site of stem cells, including the stem cells of the bone stromal lineage[75], and cells in bone such as pericytes could alter their differentiation under the influence of tumor-produced factors. Thus, tumor cells could alter the supply of osteoblastic precursors and also alter the differentiation of hematopoietic precursors into osteoclasts[22]. The animal model that is the focus of this article relies on T-cell deficient nude mice, which ignores the contribution in patients of the immune system to both normal bone cell function[76], as well as to cell-mediated immune surveillance and killing of tumor cells.

Clinical applications

The bisphosphonates are a class of drugs that resemble pyrophosphate. The replacement of the central oxygen of pyrophosphate by a carbon in the bisphosphonate backbone results in resistance to hydrolysis and confers high affinity for bone mineral, which is the basis for bisphosphonate-radionuclide conjugates as diagnostic bone-scanning agents. The bisphosphonates have high affinity for bone, where they can persist for years[77]. They are released at high concentrations in areas of active bone remodeling and are absorbed by nearby cells. They inhibit cells by several mechanisms, including the stimulation of apoptosis. Bisphosphonates are effective in animal models and the clinic. Whether bisphosphonates have significant effects *in vivo* on tumor cells or angiogenesis[78], especially at non-bone sites where their concentrations are low, is controversial.

An inhibitor of intracellular src signaling, when modified by the addition of a pair of phosphonate groups, inhibited osteoclastic bone resorption[79]. This approach could add bone specificity to existing chemotherapeutic and adjuvant compounds. Recombinant osteoprotegerin decreased osteolytic destruction and tumor burden in bone, without affecting metastases to soft-tissue sites in an animal model[59], and decreased cancer bone pain[80]. Recombinant osteoprotegerin entered clinical trials but is likely to be superceded by neutralizing antibodies against RANK ligand.

A recent study identified 6-thioguanine and 6-thioguanosine as effective inhibitors of PTHrP transcription. These agents have long been used against leukaemias and several inflammatory disorders. They were effective in animal models of humoral hypercalcemia of malignancy and breast cancer bone metastases[81]. Endothelin receptor antagonists are in extensive clinical trials, and their efficacy against osteoblastic metastasis is discussed above. Most of these adjuvant treatments target bone cells, but it may be possible to block the effects on tumors of bone-derived factors such as TGFβ[82].

Treatment options

Bisphosphonate drugs are currently approved for skeletal metastases due to multiple myeloma and solid tumors of the breast and prostate. In the last case, an anti-resorptive is effective against what are predominantly osteoblastic metastases. In fact, osteoblastic metastases are accompanied by active bone remodeling, and prostate cancer patients with bone metastases have markers of bone resorption higher than those seen in patients with osteolytic disease[83].

Bisphosphonates are also effective in animal models of osteoblastic bone metastases[84]. The results are consistent with the importance of the vicious cycle, outlined above and in Figure 1, to both osteolytic and osteoblastic diseases. The role of a vicious cycle in osteoblastic metastases is also supported by the observation that when patients with advanced metastatic prostate cancer were treated with the endothelin A receptor antagonist ABT-627, atresentan, markers of bone resorption were decreased[29,30]. Trials are now underway to test whether combining a bisphosphonate drug with an endothelin receptor antagonist is more effective than the single agent treatments.

Future directions and limitations

Areas of active research include the continuing identification of candidate osteolytic and osteoblastic factors. Many of those already identified require substantial further testing *in vivo* to determine whether they are valid targets for therapeutic intervention. They include IL-8, IL-11, CTGF, adrenomedullin, stanniocalcin, and CXCR-4. Angiogenesis is of obvious central importance in bone metastases. Many of the factors made by tumor cells are increased by hypoxia and in turn are angiogenic, in addition to having stimulatory actions on bone cells.

The roles of the abundant, bone-derived insulin-like growth factors need to be tested for their contributions to metastases to bone. IGF-2 is the most abundant bioactive factor in the mineralized matrix[1], but its role in skeletal metastasis, along with those of IGF-1, has been little studied[85]. The effects of these molecules, through activation of the type 1 IGF-1 receptor on tumor cells and bone cells, are likely to be complex and extend beyond stimulation of growth. Actions of secreted IGFs are controlled by the IGF binding proteins[86-88]. The extremely complex relationship between bone metastases and angiogenesis, discussed above, remains to be clarified.

The animal models, which are the focus of this article, have been limited to a modest number of cultured cell lines (Table 1). This is a strength in terms of defining molecular mechanisms, but it is clearly a weakness for understanding the more diverse and complex situations encountered in the clinic. We believe that this weakness is not effectively addressed by repeating the animal model experiments with more cell lines, even if funding were available for such confirmatory studies. A goal of the animal models is to provide platforms for pre-clinical testing of therapeutic interventions. If the animal models provide useful guidance in improving the care of patients with skeletal metastases, then they will have served their purpose well.

On a broader scale, are the clinical consequences of bone metastases, in particular severe bone pain and systemic weight loss (cachexia). ET-1, for example, is nociceptive. Mechanisms of bone pain are specific and under active investigation[80]. It seems likely that bone metastases release unknown factors into the circulation, which stimulate wasting of skeletal muscle[89]. These syndromes are of great consequence to the patients who suffer from cancers of the breast and prostate, which are incurable once they become housed in bone[3]. It is now appreciated that the standard treatments for patients with cancers of the breast and prostate result in bone loss. Not only does this result in skeletal morbidity for the patients, but increased bone turnover could enhance metastases to bone by stimulating the vicious cycle. Patients with treatment-related bone loss should benefit from therapy with bisphosphonate antiresorptive drugs[90]. Tumor-bone interactions, and the secreted factors which mediate them, offer targets for future therapeutic intervention to ameliorate or perhaps prevent skeletal metastases.

Acknowledgments

Work in the authors' laboratory was supported by funding from the Gerald D. Aurbach Endowment and the Mellon Institute of the University of Virginia Cancer Center, and research grants from the NIH (R01 CA69158) and the U.S. Army (DAMD17-99-1-9401) to TAG and the Veterans Administration Research Service (Merit Award) and the U.S. Army (DAMD17-98-1-8245 and DAMD17-02-1-0586) to JMC. Mr. Cliff Martin assisted in the preparation of the figure.

References

1. Hauschka PV, Mavrakos AE, Iafrati MD, Doleman SE, Klagsbrun M. Growth factors in bone matrix. Isolation of multiple types by affinity chromatography on heparin-Sepharose. J Biol Chem 1986; 261:12665-12674.
2. Chirgwin JM, Guise TA. Molecular mechanisms of tumor-bone interactions in osteolytic metastases. Crit Rev Eukaryot Gene Exp 2000; 10:159-178.
3. Mundy GR. Metastasis to bone: causes, consequences and therapeutic opportunities. Nat Rev Cancer 2002; 2:584-593.
4. Fidler IJ. The pathogenesis of cancer metastasis: the 'seed and soil' hypothesis revisited. Nat Rev Cancer 2003; 3:1-6.
5. Kang Y, Siegel PM, Shu W, Drobnjak M, Kakonen SM, Cordon-Cardo C, Guise TA, Massague J. A multigenic program mediating breast cancer metastasis to bone. Cancer Cell 2003; 3:537-549.
6. Hynes RO. Metastatic potential: generic predisposition of the primary tumor or rare, metastatic variants – or both? Cell 2003; 113:821-823.
7. Suva LJ, Winslow GA, Wettenhall RE, Hammonds RG, Moseley JM, Diefenbach-Jagger H, Rodda CP, Kemp BE, Rodriguez H, Chen EY. A parathyroid hormone-related protein implicated in malignant hypercalcemia: cloning and expression. Science 1987; 237:893-896.
8. Guise TA, Yin JJ, Taylor SD, Kumagai Y, Dallas M, Boyce BF, Yoneda T, Mundy GR. Evidence for a causal role of parathyroid hormone-related protein in the pathogenesis of human breast cancer-mediated osteoly-

sis. J Clin Invest 1996; 98:1544-1549.
9. Iguchi H, Tanaka S, Ozawa Y, Kashiwakuma T, Kimura T, Hiraga T, Ozawa H, Kono A. An experimental model of bone metastasis by human lung cancer cells: the role of parathyroid hormone-related protein in bone metastasis. Cancer Res 1996; 56:4040-4043.
10. Southby J, Kissin MW, Danks JA, Hayman JA, Moseley JM, Henderson MA, Bennett RC, Martin TJ. Immunohistochemical localization of parathyroid hormone-related protein in human breast cancer. Cancer Res 1990; 50:7710-7716.
11. Powell GJ, Southby J, Danks JA, Stillwell RG, Hayman JA, Henderson MA, Bennett RC, Martin TJ. Localization of parathyroid hormone-related protein in breast cancer metastases: increased incidence in bone compared with other sites. Cancer Res 1991; 51:3059-3061.
12. Henderson M, Danks J, Moseley J, Slavin J, Harris T, McKinlay M, Hopper J, Martin T. Parathyroid hormone-related protein production by breast cancers, improved survival, and reduced bone metastases. J Natl Cancer Inst 2001; 93:234-237.
13. Guise TA, Chirgwin JM. Transforming growth factor-beta in osteolytic breast cancer bone metastases. Clin Orthop 2003; 415(Suppl):S32-38.
14. Van der Pluijm G, Sijmons B, Vloedgraven H, Deckers M, Papapoulos S, Lowik C. Monitoring metastatic behavior of human tumor cells in mice with species-specific polymerase chain reaction: elevated expression of angiogenesis and bone resorption stimulators by breast cancer in bone metastases. J Bone Miner Res 2001; 16:1077-1091.
15. Bendre MS, Gaddy-Kurten D, Mon-Foote T, Akel NS, Skinner RA, Nicholas RW, Suva LJ. Expression of interleukin 8 and not parathyroid hormone-related protein by human breast cancer cells correlates with bone metastasis *in vivo*. Cancer Res 2002; 62:5571-5579.
16. Bendre MS, Montague DC, Peery T, Akel NS, Gaddy D, Suva LJ. Interleukin-8 stimulation of osteoclastogenesis and bone resorption is a mechanism for the increased osteolysis of metastatic bone disease. Bone 2003; 33:28-37.
17. Zhao W, Byrne MH, Boyce BF, Krane SM. Bone resorption induced by parathyroid hormone is strikingly diminished in collagenase-resistant mutant mice. J Clin Invest 1999; 103:517-524.
18. Weber GF. The metastasis gene osteopontin: a candidate target for cancer therapy. Biochim Biophys Acta 2001; 1552:61-85.
19. Carlinfante G, Vassilioul D, Svensson O, Wendel M, Heinegard D, Andersson G. Differential expression of osteopontin and bone sialoprotein in bone metastasis of breast and prostate carcinoma. Clin Exp Metastasis 2003; 20:437-444.
20. Safadi FF, Xu J, Smock SL, Kanaan RA, Selim AH, Odgren PR, Marks SC Jr, Owen TA, Popoff SN. Expression of connective tissue growth factor in bone: its role in osteoblast proliferation and differentiation *in vitro* and bone formation *in vivo*. J Cell Physiol 2003; 196:51-62.
21. Muller A, Homey B, Soto H, Ge N, Catron D, Buchanan ME, McClanahan T, Murphy E, Yuan W, Wagner SN, Barrera JL, Mohar A, Verastegui E, Zlotnik A. Involvement of chemokine receptors in breast cancer metastasis. Nature 2001; 410:50-56.
22. Roodman GD. Biology of osteoclast activation in cancer. J Clin Oncol 2001; 19:3562-3571.
23. Thomas RJ, Guise TA, Yin JJ, Elliott J, Horwood NJ, Martin TJ, Gillespie MT. Breast cancer cells interact with osteoblasts to support osteoclast formation. Endocrinology 1999; 140:4451-4458.
24. Bagi CM. Skeletal implications of prostate cancer. J Musculoskel Neuron Interact 2003; 3:112-117.
25. Nelson JB, Hedican SP, George DJ, Reddi AH, Piantadosi S, Eisenberger MA, Simons JW. Identification of endothelin-1 in the pathophysiology of metastatic adenocarcinoma of the prostate. Nat Med 1995; 1:944-949.
26. Guise TA, Yin JJ, Mohammad KS. Role of endothelin-1 in osteoblastic bone metastases. Cancer 2003; 97(3 Suppl):779-784.
27. Yin JJ, Mohammad KS, Kakonen SM, Harris S, Wu-Wong JR, Wessale JL, Padley RJ, Garrett IR, Chirgwin JM, Guise TA. A causal role for endothelin-1 in the pathogenesis of osteoblastic bone metastases. Proc Natl Acad Sci USA 2003; 100:10954-10959.
28. Rosenbaum E, Carducci MA. Pharmacotherapy of hormone refractory prostate cancer: new developments and challenges. Expert Opin Pharmacother 2003; 4:875-887.
29. Carducci MA, Padley RJ, Breul J, Vogelzang NJ, Zonnenberg BA, Daliani DD, Schulman CC, Nabulsi AA, Humerickhouse RA, Weinberg MA, Schmitt JL, Nelson JB. Effect of endothelin-A receptor blockade with atrasentan on tumor progression in men with hormone-refractory prostate cancer: a randomized, phase II, placebo-controlled trial. J Clin Oncol 2003; 21:679-689.
30. Nelson JB, Nabulsi AA, Vogelzang NJ, Breul J, Zonnenberg BA, Daliani DD, Schulman CC, Carducci MA. Suppression of prostate cancer induced bone remodeling by the endothelin receptor A antagonist atrasentan. J Urol 2003; 169:1143-1149.
31. Eaton CL, Coleman RE. Pathophysiology of bone metastases from prostate cancer and the role of bisphosphonates in treatment. Cancer Treat Rev 2003; 29:189-198.
32. Nishida T, Nakanishi T, Asano M, Shimo T, Takigawa M. Effects of CTGF/Hcs24, a hypertrophic chondrocyte-specific gene product, on the proliferation and differentiation of osteoblastic cells *in vitro*. J Cell Physiol 2000; 184:197-206.
33. Brigstock DR. The CCN family: a new stimulus package. J Endocrinol 2003; 178:169-175.
34. Maillard M, Cadot B, Ball RY, Sethia K, Edwards DR, Perbal B, Tatoud R. Differential expression of the ccn3 (nov) proto-oncogene in human prostate cell lines and tissues. Mol Pathol 2001; 54:275-280.
35. Tsai MS, Bogart DF, Li P, Mehmi I, Lupu R.

Expression and regulation of Cyr61 in human breast cancer cell lines. Oncogene 2002; 21:964-973.
36. Cornish J, Callon KE, Coy DH, Jiang NY, Xiao L, Cooper GJ, Reid IR. Adrenomedullin is a potent stimulator of osteoblastic activity *in vitro* and *in vivo*. Am J Physiol 1997; 273:E1113-1120.
37. Hamada H, Kitamura K, Chosa E, Eto T, Tajima N. Adrenomedullin stimulates the growth of cultured normal human osteoblasts as an autocrine/paracrine regulator. Peptides 2002; 23:2163-2168.
38. Cornish J, Naot D, Reid IR. Adrenomedullin - a regulator of bone formation. Regul Pept 2003; 112:79-86.
39. Zudaire E, Martinez A, Cuttitta F. Adrenomedullin and cancer. Regul Pept 2003; 112:175-183.
40. Miller MJ, Martinez A, Unsworth EJ, Thiele CJ, Moody TW, Elsasser T, Cuttitta F. Adrenomedullin expression in human tumor cell lines. Its potential role as an autocrine growth factor. J Biol Chem 1996; 271:23345-23351.
41. Rocchi P, Boudouresque F, Zamora AJ, Muracciole X, Lechevallier E, Martin PM, Ouafik L. Expression of adrenomedullin and peptide amidation activity in human prostate cancer and in human prostate cancer cell lines. Cancer Res 2001; 61:1196-1206.
42. Hastings RH, Summers-Torres D, Cheung TC, Ditmer LS, Petrin EM, Burton DW, Spragg RG, Li J, Deftos LJ. Parathyroid hormone-related protein, an autocrine regulatory factor in alveolar epithelial cells. Am J Physiol 1996; 270:L353-361.
43. Abasolo I, Yang L, Haleem R, Xiao W, Pio R, Cuttitta F, Montuenga LM, Kozlowski JM, Calvo A, Wang Z. Overexpression of adrenomedullin gene markedly inhibits proliferation of PC3 prostate cancer cells *in vitro* and *in vivo*. Mol Cell Endocrinol 2003; 199:179-187.
44. Chang AC, Jellinek DA, Reddel RR. Mammalian stanniocalcins and cancer. Endocr Relat Cancer 2003; 10:359-373.
45. Welcsh PL, Lee MK, Gonzalez-Hernandez RM, Black DJ, Mahadevappa M, Swisher EM, Warrington JA, King MC. BRCA1 transcriptionally regulates genes involved in breast tumorigenesis. Proc Natl Acad Sci USA 2002; 99:7560-7565.
46. Filvaroff EH, Guillet S, Zlot C, Bao M, Ingle G, Steinmetz H, Hoeffel J, Bunting S, Ross J, Carano RA, Powell-Braxton L, Wagner GF, Eckert R, Gerritsen ME, French DM. Stanniocalcin 1 alters muscle and bone structure and function in transgenic mice. Endocrinology 2002; 143:3681-3690
47. Yoshiko Y, Maeda N, Aubin JE. Stanniocalcin 1 stimulates osteoblast differentiation in rat calvaria cell cultures. Endocrinology 2003; 144:4134-4143.
48. Coffman JA. Runx transcription factors and the developmental balance between cell proliferation and differentiation. Cell Biol Int 2003; 27:315-324.
49. Geoffroy V, Kneissel M, Fournier B, Boyde A, Matthias P. High bone resorption in adult aging transgenic mice overexpressing cbfa1/runx2 in cells of the osteoblastic lineage. Mol Cell Biol 2002; 22:6222-6233.
50. Cramer SD, Chen Z, Peehl DM. Prostate specific antigen cleaves parathyroid hormone-related protein in the PTH-like domain: inactivation of PTHrP-stimulated cAMP accumulation in mouse osteoblasts. J Urol 1996; 156:526-531.
51. Iwamura M, Hellman J, Cockett AT, Lilja H, Gershagen S. Alteration of the hormonal bioactivity of parathyroid hormone-related protein (PTHrP) as a result of limited proteolysis by prostate-specific antigen. Urology 1996; 48:317-325.
52. Schluter KD, Katzer C, Piper HM. A N-terminal PTHrP peptide fragment void of a PTH/PTHrP-receptor binding domain activates cardiac ET(A) receptors. Br J Pharmacol 2001; 132:427-432.
53. Ruchon AF, Marcinkiewicz M, Ellefsen K, Basak A, Aubin J, Crine P, Boileau G. Cellular localization of neprilysin in mouse bone tissue and putative role in hydrolysis of osteogenic peptides. J Bone Miner Res 2000; 15:1266-1274.
54. Wakefield LM, Roberts AB. TGF-beta signaling: positive and negative effects on tumorigenesis. Curr Opin Genet Dev 2002; 12:22-29.
55. Yin JJ, Selander KS, Chirgwin JM, Dallas M, Grubbs BG, Wieser R, Massague J, Mundy GR, Guise TA. TGFβ signaling blockade inhibits parathyroid hormone-related protein secretion by breast cancer cells and bone metastases development. J Clin Invest 1999; 103:197-206.
56. Kakonen SM, Selander KS, Chirgwin JM, Yin JJ, Burns S, Rankin WA, Grubbs BG, Dallas M, Cui Y, Guise TA. Transforming growth factor-beta stimulates parathyroid hormone-related protein and osteolytic metastases via Smad and mitogen-activated protein kinase signaling pathways. J Biol Chem 2002; 277:24571-24578.
57. Dallas SL, Rosser JL, Mundy GR, Bonewald LF. Proteolysis of latent transforming growth factor-beta (TGF-β)-binding protein-1 by osteoclasts. A cellular mechanism for release of TGF-beta from bone matrix. J Biol Chem 2002; 277:21352-21360.
58. Sasaki A, Boyce BF, Story B, Wright KR, Chapman M, Boyce R, Mundy GR, Yoneda T. Bisphosphonate risedronate reduces metastatic human breast cancer burden in bone in nude mice. Cancer Res 1995; 55:3551-3557.
59. Morony S, Capparelli C, Sarosi I, Lacey DL, Dunstan CR, Kostenuik PJ. Osteoprotegerin inhibits osteolysis and decreases skeletal tumor burden in syngeneic and nude mouse models of experimental bone metastasis. Cancer Res 2001; 61:4432-4436.
60. Orr W, Varani J, Gondex MK, Ward PA, Mundy GR. Chemotactic responses of tumor cells to products of resorbing bone. Science 1978; 203:176-179.
61. Roudier MP, True LD, Higano CS, Vesselle H, Ellis W, Lange P, Vessella RL. Phenotypic heterogeneity of end-stage prostate carcinoma metastatic to bone. Hum Pathol 2003; 34:646-653.

62. Bagnato A, Spinella F. Emerging role of endothelin-1 in tumor angiogenesis. Trends Endocrinol Metab 2003; 14:44-50.
63. Martinez A, Vos M, Guedez L, Kaur G, Chen Z, Garayoa M, Pio R, Moody T, Stetler-Stevenson WG, Kleinman HK, Cuttitta F. The effects of adrenomedullin overexpression in breast tumor cells. J Natl Cancer Inst 2002; 94:1226-1237.
64. Belperio JA, Keane MP, Arenberg DA, Addison CL, Ehlert JE, Burdick MD, Strieter RM. CXC chemokines in angiogenesis. J Leukoc Biol 2000; 68:1-8.
65. Menendez JA, Mehmi I, Griggs DW, Lupu R. The angiogenic factor CYR61 in breast cancer: molecular pathology and therapeutic perspectives. Endocr Relat Cancer 2003; 10:141-152.
66. Zlot C, Ingle G, Hongo J, Yang S, Sheng Z, Schwall R, Paoni N, Wang F, Peale FV Jr, Gerritsen ME. Stanniocalcin 1 is an autocrine modulator of endothelial angiogenic responses to hepatocyte growth factor. J Biol Chem 2003; 278:47654-47659.
67. Bakre MM, Zhu Y, Yin H, Burton DW, Terkeltaub R, Deftos LJ, Varner JA. Parathyroid hormone-related peptide is a naturally occurring, protein kinase A-dependent angiogenesis inhibitor. Nat Med 2002; 8:995-1003.
68. Wykoff CC, Pugh CW, Maxwell PH, Harris AL, Ratcliffe PJ. Identification of novel hypoxia dependent and independent target genes of the von Hippel-Lindau (VHL) tumour suppressor by mRNA differential expression profiling. Oncogene 2000; 19:6297-6305.
69. Garayoa M, Martinez A, Lee S, Pio R, An WG, Neckers L, Trepel J, Montuenga LM, Ryan H, Johnson R, Gassmann M, Cuttitta F. Hypoxia-inducible factor-1 (HIF-1) up-regulates adrenomedullin expression in human tumor cell lines during oxygen deprivation: a possible promotion mechanism of carcinogenesis. Mol Endocrinol 2000; 14:848-862.
70. Kunz M, Moeller S, Koczan D, Lorenz P, Wenger RH, Glocker MO, Thiesen HJ, Gross G, Ibrahim SM. Mechanisms of hypoxic gene regulation of angiogenesis factor Cyr61 in melanoma cells. J Biol Chem 2003; 278:45651-45660.
71. Shimo T, Kubota S, Kondo S, Nakanishi T, Sasaki A, Mese H, Matsumura T, Takigawa M. Connective tissue growth factor as a major angiogenic agent that is induced by hypoxia in a human breast cancer cell line. Cancer Lett 2001; 174:57-64.
72. Lal A, Peters H, St Croix B, Haroon ZA, Dewhirst MW, Strausberg RL, Kaanders JH, van der Kogel AJ, Riggins GJ. Transcriptional response to hypoxia in human tumors. J Natl Cancer Inst 2001; 93:1337-1343.
73. Cooper CR, McLean L, Walsh M, Taylor J, Hayasaka S, Bhatia J, Pienta KJ. Preferential adhesion of prostate cancer cells to bone is mediated by binding to bone marrow endothelial cells as compared to extracellular matrix components *in vitro*. Clin Cancer Res 2000; 6:4839-4847.
74. Di Raimondo F, Azzaro MP, Palumbo G, Bagnato S, Giustolisi G, Floridia P, Sortino G, Giustolisi R. Angiogenic factors in multiple myeloma: higher levels in bone marrow than in peripheral blood. Haematologica 2000; 85:800-805.
75. Bianco P, Riminucci M, Gronthos S, Robey PG. Bone marrow stromal stem cells: nature, biology, and potential applications. Stem Cells 2001; 19:180-192.
76. Martin TJ, Romas E, Gillespie MT. Interleukins in the control of osteoclast differentiation. Crit Rev Eukaryot Gene Expr 1998; 8:107-123
77. Russell RG, Rogers MJ. Bisphosphonates: from the laboratory to the clinic and back again. Bone 1999; 5:97-106.
78. Green JR. Antitumor effects of bisphosphonates. Cancer 2003; 97(Suppl.3):840-847.
79. Shakespeare W, Yang M, Bohacek R, Cerasoli F, Stebbins K, Sundaramoorthi R, Azimioara M, Vu C, Pradeepan S, Metcalf C III, Haraldson C, Merry T, Dalgarno D, Narula S, Hatada M, Lu X, van Schravendijk MR, Adams S, Violette S, Smith J, Guan W, Bartlett C, Herson J, Iuliucci J, Weigele M, Sawyer T. Structure-based design of an osteoclast-selective, nonpeptide src homology 2 inhibitor with *in vivo* anti-resorptive activity. Proc Natl Acad Sci USA 2000; 97:9373-9378.
80. Mantyh PW, Clohisy DR, Koltzenburg M, Hunt SP. Molecular mechanisms of cancer pain. Nat Rev Cancer 2002; 2:201-209.
81. Gallwitz WE, Guise TA, Mundy GR. Guanosine nucleotides inhibit different syndromes of PTHrP excess caused by human cancers *in vivo*. J Clin Invest 2002; 110:1559-1572.
82. Dumont N, Arteaga CL. Targeting the TGFβ signaling network in human neoplasia. Cancer Cell 2003; 3:531-536.
83. Guise TA, Chirgwin JM. Role of bisphosphonates in prostate cancer bone metastases. Semin Oncol 2003; 30:717-723.
84. Corey E, Brown LG, Quinn JE, Poot M, Roudier MP, Higano CS, Vessella RL. Zoledronic acid exhibits inhibitory effects on osteoblastic and osteolytic metastases of prostate cancer. Clin Cancer Res 2003; 9:295-306.
85. Jackson JG, Zhang X, Yoneda T, Yee D. Regulation of breast cancer cell motility by insulin receptor substrate-2 (IRS-2) in metastatic variants of human breast cancer cell lines. Oncogene 2001; 20:7318-7325.
86. Mohan S, Baylink DJ. IGF-binding proteins are multifunctional and act via IGF-dependent and-independent mechanisms. J Endocrinol 2002; 175:19-31.
87. Firth SM, Baxter RC. Cellular actions of the insulin-like growth factor binding proteins. Endocr Rev 2002; 23:824-854.
88. LeRoith D, Roberts CT Jr. The insulin-like growth factor system and cancer. Cancer Lett 2003; 195:127-137.
89. Tisdale MJ. Cachexia in cancer patients. Nat Rev Cancer 2002; 2:862-871.
90. Smith MR. Bisphosphonates to prevent skeletal complications in men with metastatic prostate cancer. J Urol 2003; 170:S55-57.

91. Cornish J, Callon KE, Bava U, Coy DH, Mulvey TB, Murray MA, Cooper GJ, Cooper GJ, Reid IR. Systemic administration of adrenomedullin (27-52) increases bone volume and strength in male mice. J Endocrinol 2001; 170:251-257.
92. Miki T, Yano S, Hanibuchi M, Kanematsu T, Muguruma H, Sone S. Parathyroid hormone-related protein (PTHrP) is responsible for production of bone metastasis, but not visceral metastasis, by human small cell lung cancer SBC-5 cells in natural killer cell-depleted SCID mice. Int J Cancer 2004; 108:511-515.
93. Chiao JW, Moonga BS, Yang YM, Kancherla R, Mittelman A, Wu-Wong JR, Ahmed T. Endothelin-1 from prostate cancer cells is enhanced by bone contact which blocks osteoclastic bone resorption. Br J Cancer 2000; 83:360-365.
94. Dall'Era MA, Shih SJ, Yang J, Benik S, Gandour-Edwards R, Evans CP. Differential expression of angiogenic cytokines by cell lines and primary cultures of human prostate cancer. Prostate Cancer Prostatic Dis 2001; 4:106-111.
95. Scott PA, Gleadle JM, Bicknell R, Harris AL. Role of the hypoxia sensing system, acidity and reproductive hormones in the variability of vascular endothelial growth factor induction in human breast carcinoma cell lines. Int J Cancer 1998; 75:706-712.
96. Corey E, Quinn JE, Bladou F, Brown LG, Roudier MP, Brown JM, Buhler KR, Vessella RL. Establishment and characterization of osseous prostate cancer models: intra-tibial injection of human prostate cancer cells. Prostate 2002; 52:20-33
97. Yi B, Williams PJ, Niewolna M, Wang Y, Yoneda T. Tumor-derived platelet-derived growth factor-BB plays a critical role in osteosclerotic bone metastasis in an animal model of human breast cancer. Cancer Res 2002; 62:917-923.

doi:10.1016/j.jmb.2004.07.085 J. Mol. Biol. (2004) 342, 847–860

JMB

Available online at www.sciencedirect.com

SCIENCE DIRECT®

ELSEVIER

The Crystal Structure of Mouse Phosphoglucose Isomerase at 1.6 Å Resolution and its Complex with Glucose 6-Phosphate Reveals the Catalytic Mechanism of Sugar Ring Opening

J.T. Graham Solomons[1], Ella M. Zimmerly[1], Suzanne Burns[2] N. Krishnamurthy[1], Michael K. Swan[1], Sandra Krings[1], Hilary Muirhead[3] John Chirgwin[4] and Christopher Davies[1]*

[1]*Department of Biochemistry and Molecular Biology, Medical University of South Carolina Charleston, SC 29425, USA*

[2]*Research Service, Veterans Administration Medical Center San Antonio, TX 78230, USA*

[3]*School of Medical Sciences University of Bristol, Bristol BS8 1TD, UK*

[4]*Department of Medicine University of Virginia Charlottesville, VA 22908 USA*

**Corresponding author*

Phosphoglucose isomerase (PGI) is an enzyme of glycolysis that interconverts glucose 6-phosphate (G6P) and fructose 6-phosphate (F6P) but, outside the cell, is a multifunctional cytokine. High-resolution crystal structures of the enzyme from mouse have been determined in native form and in complex with the inhibitor erythrose 4-phosphate, and with the substrate glucose 6-phosphate. In the substrate-bound structure, the glucose sugar is observed in both straight-chain and ring forms. This structure supports a specific role for Lys518 in enzyme-catalyzed ring opening and we present a "push–pull" mechanism in which His388 breaks the O5–C1 bond by donating a proton to the ring oxygen atom and, simultaneously, Lys518 abstracts a proton from the C1 hydroxyl group. The reverse occurs in ring closure. The transition from ring form to straight-chain substrate is achieved through rotation of the C3–C4 bond, which brings the C1–C2 region into close proximity to Glu357, the base catalyst for the isomerization step. The structure with G6P also explains the specificity of PGI for glucose 6-phosphate over mannose 6-isomerase (M6P). To isomerize M6P to F6P requires a rotation of its C2–C3 bond but in PGI this is sterically blocked by Gln511.

Keywords: phosphoglucoseisomerase; aldose-ketose isomerase; enzyme mechanism; cytokine; X-ray crystallography

Introduction

Phosphoglucose isomerase (PGI; EC 5.3.1.9) catalyses the interconversion of glucose 6-phosphate (G6P) and fructose 6-phosphate (F6P), a reaction with direct roles in glycolysis and gluconeogenesis and, indirectly, other branches of carbohydrate metabolism such as the pentose phosphate pathway. In addition to its enzymatic activity, PGI acts as a cytokine in a wide variety of extracellular activities,[1–3] and hence the enzyme now carries many names, including that of autocrine motility factor (AMF) and maturation factor (MF), but how the protein functions in this context is unclear. PGI is better characterised as an enzyme, but some key aspects of its catalytic mechanism remain unresolved, and these are addressed here.

PGI belongs to the aldose-ketose isomerase family of enzymes, all of which transfer a hydrogen atom between C1 and C2 of their respective substrates. This hydrogen atom can move by one of two mechanisms: as a proton *via* a *cis*-enediol/*cis*-enediolate intermediate or more directly as a hydride.[4] The existence of the *cis*-enediol mechanism

Present address: N. Krishnamurthy, Biology Department, Brookhaven National Laboratory Upton, NY 11973-5000, USA.

Abbreviations used: PAB, 5-phosphoarabinonate; AMF, autocrine motility factor; βME, β-mercaptoethanol; E4P, erythrose 4-phosphate; EST, expressed sequence tag; F6P, fructose 6-phosphate; G6P, glucose 6-phosphate; MF, maturation factor; mPGI, mouse phosphoglucose isomerase; PGI, phosphoglucose isomerase; PGI/PMI, phosphoglucose isomerase/phosphomannose isomerase; rms, root-mean-square; rPGI, rabbit phosphoglucose isomerase.

E-mail address of the corresponding author: davies@musc.edu

0022-2836/$ - see front matter

is well established for PGI,[4] but for many years, the identity of the enzymatic base responsible for proton abstraction from C2 of G6P or C1 of F6P was unknown. Recent determination of the crystal structures of PGI from mammalian sources, however, have led to proposals that Glu357 is responsible.[5,6]

In contrast to other aldose-ketose isomerases, such as triose phosphate isomerase, PGI uses a sugar substrate that exists in solution overwhelmingly in the hemiacetal or hemiketal ring form,[7] and indeed, a crystal structure of rabbit PGI in complex with F6P shows the substrate bound in the ring form.[8] But for proton transfer to occur between C1 and C2, the substrate must be in the open-chain form and, hence, the enzyme catalyzes a second activity, that of ring opening. In agreement with this, crystal structures of inhibitor-bound PGIs show the ligand to be in the open-chain conformation.[6,9,10] The nearest residues to the sugar ring oxygen atom are His388 and Lys518 (mammalian numbering), and, of these, histidine is most likely to act as an acid catalyst in ring opening but how the lysine residue contributes to this process, if at all, is unknown.

Another unresolved issue in the catalytic functioning of PGI is how the enzyme permits rotation of the substrate within the active site without compromising specificity. Such a rotation must occur after the ring-opening step in order to bring the C1–C2 region of the substrate in close proximity to Glu357 for isomerisation. A similar rotation might occur during the anomerisation of its substrates (a third enzyme activity for PGI). In principle, such rotations when coupled with isomerization could generate mannose 6-phosphate.[11] However, PGI is essentially specific for F6P and G6P, and it will not isomerase mannose 6-phosphate to F6P except at an extremely slow and non-physiological rate.[1] Interestingly, distantly related members of the PGI superfamily from certain Archaea do show dual phosphoglucose/phosphomannose isomerase (PGI/PMI) activities[12] but how "conventional" PGI prevents the epimerisation of G6P to M6P is unknown.

Here, we present a series of high-resolution crystal structures of PGI derived from mouse. These include complexes with the inhibitor erythrose 4-phosphate and with the substrate, glucose 6-phosphate. The complex with G6P provides unique insight because in this structure the substrate is present in both the open-chain form and the ring form. Together, these data permit a definitive and comprehensive description of the catalytic mechanism of this interesting multifunctional enzyme.

Results

Structure determination

Phosphoglucose isomerase from mouse crystallized relatively easily over wells containing 1.6–2.1 M ammonium sulphate buffered in the pH range 6.5–9.5. The native crystal used in this study was harvested from 1.9 M ammonium sulphate, 100 mM Tris–HCl (pH 8.5). The crystals grow as large plates of approximate dimensions 1 mm × 1 mm × 0.2 mm and were typically cut into smaller pieces for data collection. Initial diffraction analysis revealed that the crystals belong to space group $P2$ or $P2_1$ with cell dimensions $a=69.2$ Å, $b=116.1$ Å, $c=73.1$ Å and $\beta=101.3°$. An estimate of the solvent content (46.2%, v/v) indicated that the asymmetric unit of these crystals is a dimer of PGI,[13] which corresponds to the biological form of this enzyme. A complete dataset extending to 1.6 Å resolution was collected (Table 1) and examination of the systematic absences revealed the space group to be $P2_1$. The structure was solved by molecular replacement and refined to a crystallographic R-factor of 21.2% (R_{free} 24.5%) with excellent stereochemistry. The final model comprises two PGI subunits (residues 1–556), 1017 water molecules as well as molecules of sulphate, β-mercaptoethanol (βME) and glycerol, derived from the crystallization solution. For both subunits, only the methionine at the N terminus and the C-terminal residue are not visible in the electron density map.

Structure description

As expected, the fold of mouse PGI is essentially the same as PGIs from other mammalian sources[5,9,14,15] and, hence, will be described only briefly. Each subunit comprises two domains of nearly equal size, but historically these have been termed small and large. The small domain is built around a five-stranded parallel β sheet, whereas the large domain contains a mixed six-stranded parallel/antiparallel β sheet. Both sheets are packed on both sides by α helices. Two interesting features of this fold are a "hook" comprising residues 440–465 and a 45 residue extension at the C terminus, both of which make extensive interactions with the partner subunit in the dimer. The active site comprises highly conserved residues, including Glu357, His388 and Lys518, all of which have a role in catalysis. The histidine residue belongs to the partner subunit of the dimer and thus the active site is comprised of protein chains from both subunits.

The two subunits in the dimer superimpose closely with an rms deviation between all main-chain atoms of 0.93 Å. The only structural differences of significance map to the active-site regions, which correlate with the binding of species from the crystallization solution, and there is a slight shift in the relative position of the hook structure. In molecule A, the active site contains one sulphate ion, which occupies the same position as the phosphate group of the substrate molecules for PGI. There is some electron density located between threonine residues 211 and 214 and Lys518, which might be a molecule of βME. The view in the active site of molecule B is different: two sulphate ions

Table 1. X-ray diffraction data and refinement statistics

A. *Data collection*	Native	E4P	G6P
Concentration of soak (mM)	–	5	5
Time of soak (minutes)	–	90	45
Resolution range (Å)	50–1.6 (1.66–1.60)	54–1.7 (1.76–1.70)	45–1.6 (1.66–1.6)
R_{merge} (%)	7.5 (42.2)	6.7 (27.1)	5.7 (36.9)
Redundancy	7.3 (5.9)	4.2 (3.0)	6.0 (2.8)
Completeness (%)	99.5 (96.4)	97.5 (81.8)	94.7 (79.9)
$\langle I \rangle / \langle \sigma I \rangle$	5.4 (1.5)	7.4 (1.9)	34.1 (3.1)
B. *Refinement*			
Resolution range (Å)	15.0–1.6	50.0–1.7	45–1.6
Sigma cut-off applied	0.0	0.0	0.0
No. total reflections used	146,126	118,864	143,578
No. β-mercaptoethanol molecules	5	6	1
No. glycerol molecules	7	6	12
No. sulphate molecules	10	7	8
No. water molecules	1017	832	858
R-factor (%)	21.3	19.2	17.9
R_{work} (%)	21.1	19.0	17.8
R_{free} (%)	24.6	21.5	20.7
rms deviations from ideal stereochemistry			
Bond lengths (Å)	0.010	0.008	0.011
Bond angles (deg.)	1.16	1.05	1.21
Overall *B*-factor (Å^2)	24.4	19.1	23.8
Mean *B*-factor (main-chain) (Å^2)	22.4	17.7	21.7
rms deviation in main-chain *B* factor (Å^2)	0.42	0.31	0.45
Mean *B*-factor (side-chains and water molecules) (Å^2)	26.1	20.3	25.6
rms deviation in side-chain *B*-factors (Å^2)	1.31	1.01	1.39
Ramachandran plot			
Residues in most-favoured region (%)	89.4	90.0	89.1
Residues in additionally allowed regions (%)	10.6	9.8	10.9
Residues in generously allowed regions (%)	0.0	0.1	0.0
Residues in disallowed regions (%)	0.0	0.1	0.0

$R_{merge} = \sum |I_i - I_m| / \sum I_i$, where I_i is the intensity of the *i*th measured reflection and I_m is the mean intensity of all symmetry-related reflections. Figures within parentheses are for the outer-resolution shell.

have bound and neither overlaps with the phosphate-binding site. One is in approximately the same position as the βME-like density in monomer A, whereas the other occupies a unique position adjacent to Gly158, Gln353 and Glu357, which corresponds approximately with the site of hydrogen transfer during the isomerase reaction.

When comparing previous structures of PGI from mammalian sources, we have noted a conformational change within the small domain of the protein induced by the binding of substrate,[14] and in the case of human PGI, by sulphate alone.[5] In both cases, either the phosphate group of the sugar substrate or a sulphate ion occupying that position induces a closure of some elements of the small domain around the phosphate-binding site. Interestingly, in the structure of mouse PGI, both open and closed forms are present (Figure 1). In molecule A, the sulphate ion occupies the phosphate-binding site and the conformation is closed, whereas in molecule B, although two molecules of sulphate have bound, none overlaps with the phosphate-binding site and hence the conformation is open.

Complex with erythrose 4-phosphate

Erythrose 4-phosphate (E4P) is a well-known inhibitor of PGI with a K_i of 0.7 μM against the enzyme isolated from rabbit muscle.[16] The structure of mouse PGI in complex with E4P was determined to 1.7 Å resolution (Table 1). This structure refined with a better agreement between the model and data than the native structure and has an *R*-factor of 19.1% (R_{free} 21.5%). Density corresponding to bound E4P was clear at both active sites (Figure 2). Since the phosphate-binding site of molecule B is now occupied by a phosphate group, the conformation of the small domain has now switched to a closed conformation when compared to the native enzyme. Hence, the contacts made by E4P are essentially the same in both active sites of the dimer. As expected, other known conformational changes in response to ligand binding have occurred. These are of the 3_{10} helix comprising residues 383–389, and a section of helix α23 comprising residues 512–522. Both of these bring highly conserved amino acids, His338 and Lys518, respectively, toward the active site when compared with the sulphate-bound "native" structure. The same structural changes have been observed in other mammalian PGIs.[10,14,15,17]

Numerous enzyme–ligand contacts contribute to the binding of E4P (Figure 2). The side-chains of Ser159, Ser209, Thr211, Thr214 and the backbone amide groups of Lys210 and Thr211, as well as several water molecules, orient the phosphate group. Lys518 contacts both O3 and O4 of the inhibitor, and O3 is contacted by His388. O2 contacts the amide group of Gly158 and a water molecule. The positions of oxygen atoms O2, O3

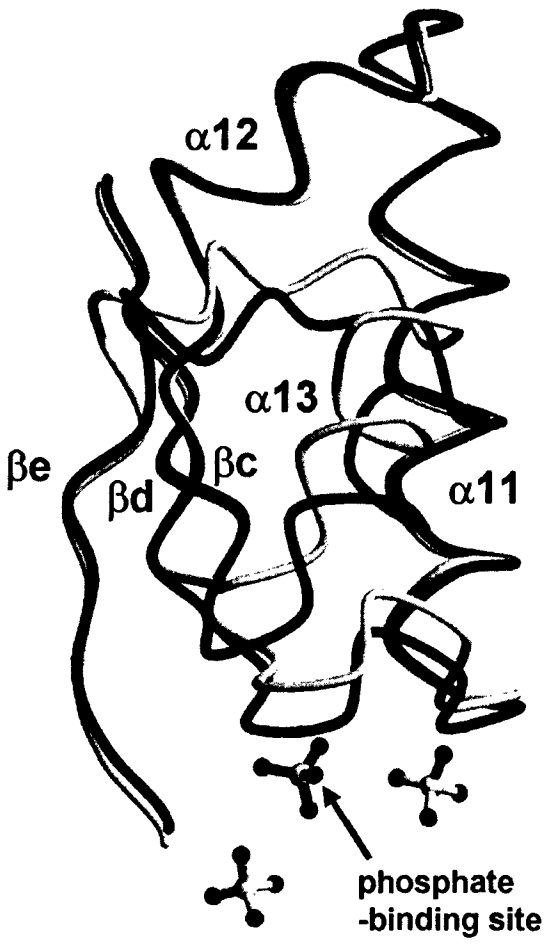

Figure 1. Conformational differences between the two subunits of mouse PGI caused by binding of sulphate ions from the crystallization solution. This superimposition of the protein backbones of the enzyme shows a section of the small domain near the active site that exists in both "open" and "closed" forms. The backbone of molecule A is coloured blue and that of molecule B is grey. The sulphate ions are shown in ball-and-stick format in which the bonds are the same colour as their respective subunits. The elements of secondary structure are labeled according to human PGI.[5] This Figure was prepared using MOLSCRIPT[35] and Raster3D.[36]

and O4 overlap very closely with those of water molecules in the native structure. The most interesting aspect of the binding, however, is the apparent dual position of O1. During refinement of the crystal structure, a peak of density in the $|F_o|-|F_c|$ electron density map adjacent to C1 indicated that the O1 atom occupied two alternative conformations, termed O1(A) and O1(B). This was observed in both subunits of the enzyme. A series of refinements showed that the magnitude of the $|F_o|-|F_c|$ peaks were reduced most when these positions were each assigned an occupancy of 50% (in both subunits). O1(A) contacts the side-chains of Glu357 and Gln353, and the main-chain amide group of Gly158. O1(B) also contacts Glu357 and makes a water-mediated contact with Arg272. Although not charged, this inhibitor mimics spatially a carboxylate group, and therefore its mode of inhibition may actually be very similar to other inhibitors of PGI, such as 6-phosphogluconate (6PG) and 5-phosphoarabinonate (PAB), which are carboxylic acids and not aldoses.

Complex with glucose 6-phosphate

Crystals of mouse PGI were soaked in 5 mM fructose 6-phosphate for 45 minutes, and a dataset extending to 1.6 Å was collected on a synchrotron source. After a single round of refinement, density corresponding to a bound substrate was observed in the active site of molecule A. Initially, an attempt was made to model this density as fructose 6-phosphate, but it soon became apparent that the ring-shaped density could accommodate only a six-membered sugar ring, rather than five, and hence glucose 6-phosphate was modeled instead. The tight fit of the G6P ring within the density suggests that the ring bond (O5–C1) may be broken, but this level of detail cannot be resolved unambiguously at the current resolution of the data. Irrespective, it is clear that, in this crystalline form of the PGI dimer, one of the active sites is catalytically competent and has converted F6P to G6P. After further rounds of refinement, persistent $|F_o|-|F_c|$ density remained that was contiguous with that of the substrate. The only interpretation for this density was that a proportion of glucose 6-phosphate was present in the open-chain form. Hence, the final structure contains glucose 6-phosphate in both ring and open-chain forms, each assigned an occupancy of 70% and 30%, respectively. The atoms of each form of the sugar refined to reasonable *B* values, comparable with the overall *B* value of the structure, and both the positive and the negative contours of the $|F_o|-|F_c|$ difference density contain only minor peaks, supporting the interpretation of the electron density. Unbiased electron density within the active site, corresponding to these two forms of G6P, is shown in Figure 3(a). At the current resolution, the electron density cannot distinguish a distinct conformer for the sugar ring of G6P and suggests a mixed population of boat and chair forms.

Unlike the structure in complex with E4P, the view of the two active sites in the mPGI–G6P complex structure is different because G6P has bound only to the active site of molecule A. The active site of molecule B appears to be occupied instead by two molecules of sulphate: the stronger of these, as evidenced by the electron density and the refined *B* values, is in the same position as the substrate phosphate-binding site and the other weaker site lies close to Gly158 and Glu357. Thus, in molecule B, the pattern of sulphate binding has changed somewhat between the G6P-soaked and sulphate-bound "native" structures. The same

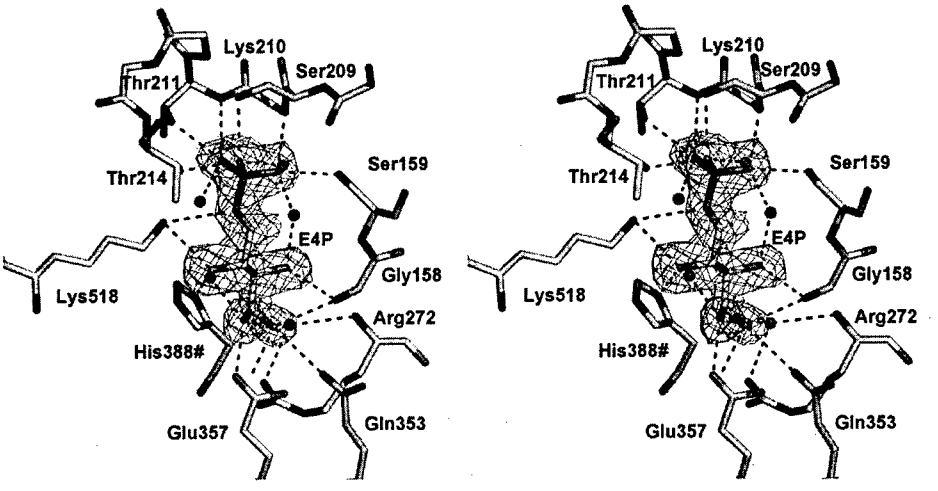

Figure 2. The structure of mouse PGI in complex with erythrose 4-phosphate (E4P) at 1.7 Å resolution. A stereo picture of the active site region, showing unbiased $|F_o|-|F_c|$ electron density of the bound inhibitor, contoured at 1 σ and coloured blue. The active-site residues and E4P are shown in bond form. Water molecules are represented as red spheres and potential hydrogen bonds are shown as broken lines. This shows the active site of molecule A but the view in molecule B is the same. The hash (#) denotes that a residue comes from the adjacent subunit. This Figure was prepared using Pymol (http://pymol.sourceforge.net/).

sulphate molecule near Gly158 and Glu357 is seen in both structures but in the G6P-bound structure, a new sulphate molecule now occupies the phosphate-binding site. As discussed below, it is possible that these peaks of density correspond instead to a molecule of G6P bound with low occupancy.

For molecule A, the contacts between both forms of G6P and the active site residues are depicted in Figure 3(b) and (c). The phosphate group is positioned by the same cluster of threonine residues, serine residues and main-chain amide groups as described above for E4P. Other interactions, however, depend on the conformation of the ligand. The most striking of these concerns the different positions of the C1–C2 region of the substrate. In the ring form, this region of the substrate is near His388, whereas in the straight-chain form it is positioned on the opposite site of the active site in a pocket formed by Gln511, Gly271, Arg272 and Glu357. In this position, the $O^{\varepsilon 2}$ atom of the carboxyl group of Glu357 lies approximately equidistant between C1 and C2. Moreover, in straight-chain form, the C1 hydroxyl group contacts Glu357 and both the main-chain amide and side-chain guanidinium group of Arg272, but the same oxygen atom in the ring form is located some 6.9 Å away on the other side of the active site, where it is tethered by Lys518. When the ring form is present, a water molecule instead occupies the same position as O1 in the straight-chain form. These two distinct binding modes for G6P are direct evidence of a large shift in the conformation of the substrate that occurs after the ring-opening step (discussed below). Within the ring form itself, O1 appears to occupy two positions and these could correspond to the two anomers of the substrate. The oxygen atom in the α-like position is close to a water molecule, and that in the β-like position is near the N^{ζ} atom of Lys518. The position of the C2 hydroxyl group also differs between the two binding modes: it hydrogen bonds with a water molecule in the straight chain, but in the ring form contacts Glu357. Continuing along the substrate chain, the C3 hydroxyl group in the ring form occupies the same position at C3 in the straight form and is within hydrogen bonding distance of Glu357. In the straight-chain form, however, this group hydrogen bonds instead with the carbonyl group of His388. Thereafter, the remaining atoms of the substrate converge. The position of the C4 hydroxyl group in both forms is essentially the same and makes potential hydrogen bonds with the main-chain amide group of Gly158 and a water molecule. Likewise, the C5 hydroxyl group in the open-chain form and its ring oxygen counterpart occupy the same position.

The binding of G6P to the active site of molecule A produces almost no shifts in the positions of the amino acid residues surrounding the substrate molecule compared to the same subunit in the substrate-free structure (not shown). This is in contrast to the situation in the E4P complex, where the binding of that ligand causes a large movement of α23 such that both the N^{ζ} atom of Lys518 and $N^{\delta 2}$ atom of His388 are equidistant from the ring oxygen atom. In the complex with G6P, the $N^{\delta 2}$ atom of His388 is 2.8 Å from the ring oxygen atom, but the N^{ζ} atom of Lys518 remains 4.6 Å away. This has implications for the mechanism of sugar ring opening (discussed below).

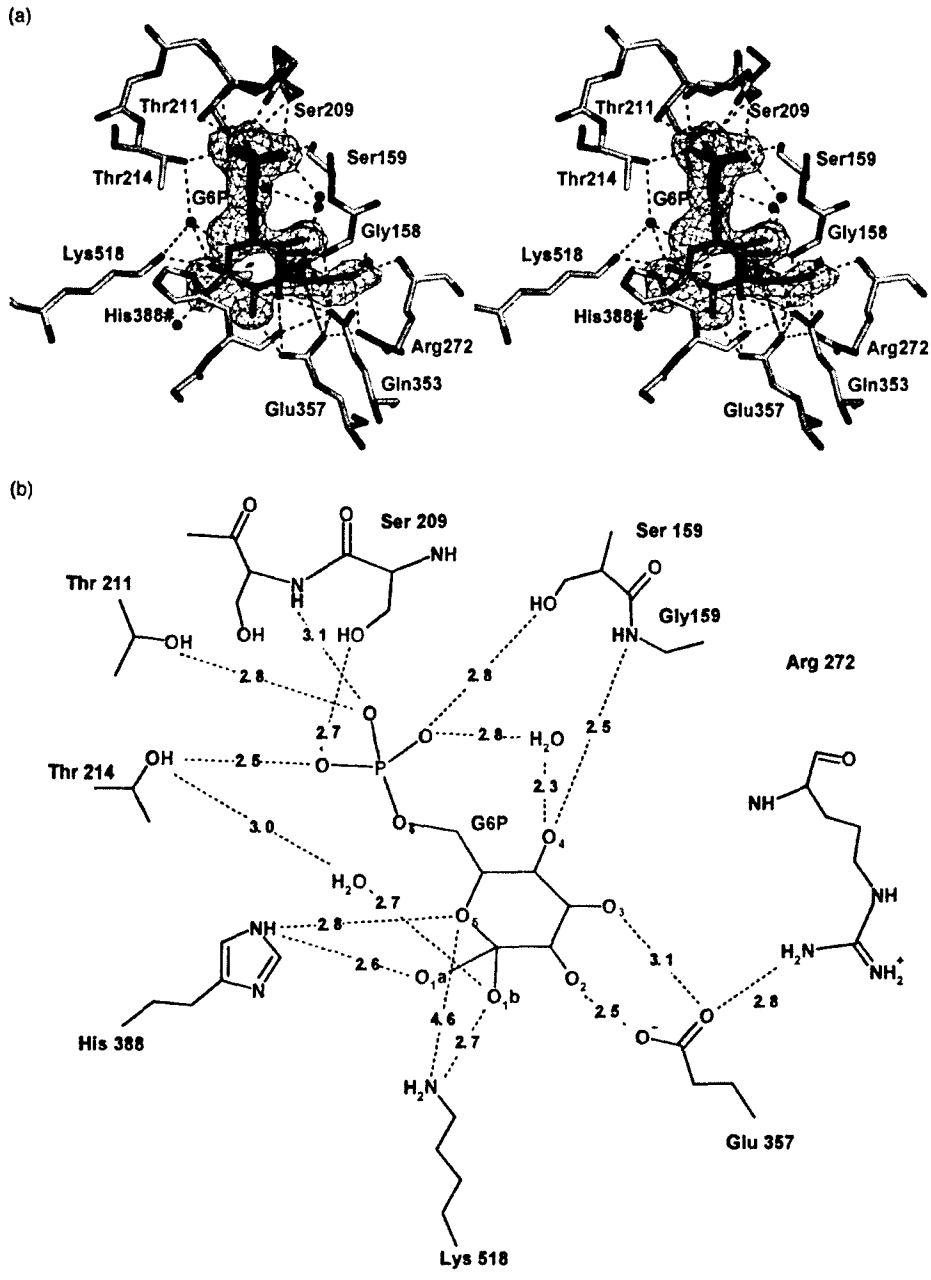

Figure 3 (*legend opposite*)

Comparison with rabbit PGI structure complexed with fructose-6-phosphate

The structure of mouse PGI in complex with G6P was compared with a published structure of rabbit PGI in complex with ring-form F6P.[8] The two structures superimpose with an rms deviation in all main-chain atoms of 0.47 Å (molecule A of mouse PGI *versus* molecule A of rabbit PGI) and, most importantly, the individual positions of residues in the two active sites overlap very closely (Figure 4). In fact, surprisingly, most of the divergence between the active sites is in the substrate itself and not the protein structure, due primarily to the altered shape of a five-membered furanose *versus* a six-membered pyranose ring. Overall, the enzyme contacts made by G6P and F6P, both in the ring form, are quite similar. There is some difference in the position of C6, but the phosphate-binding contacts and the contacts involving the C3 and C4 hydroxyl groups of both G6P and F6P are essentially the same in both structures. The principal differences occur in the C1–C2 regions of the substrates. In essence, the relative positions of

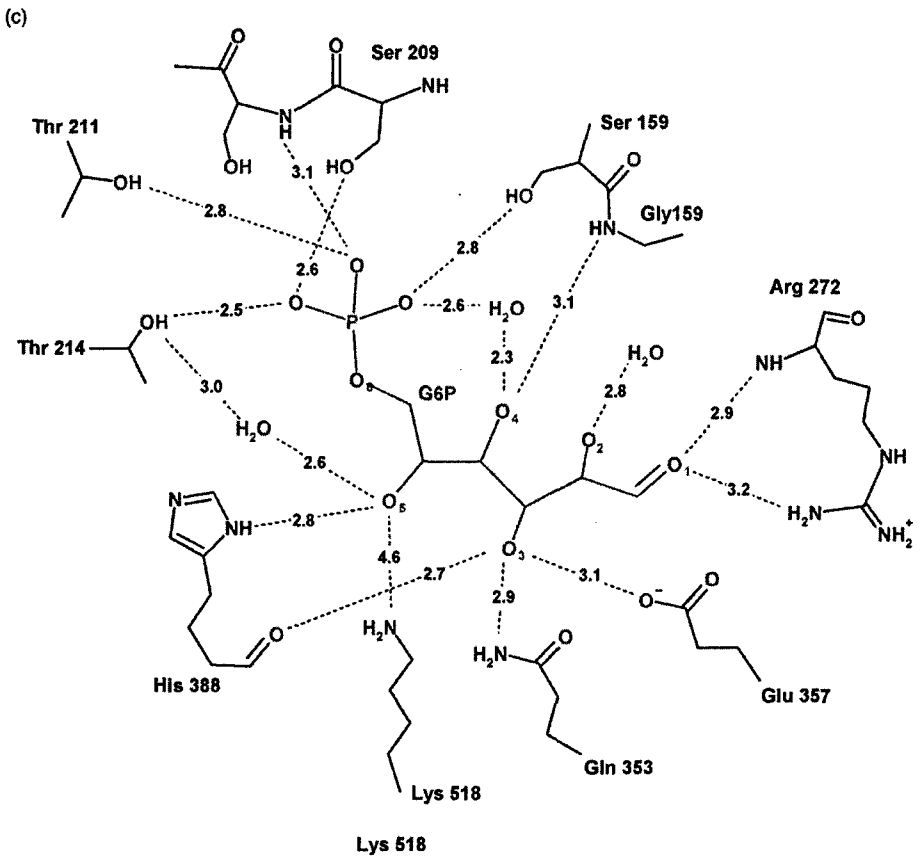

Figure 3. The structure of mouse PGI in complex with glucose 6-phosphate at 1.6 Å resolution. (a) A stereo picture of the active site region of molecule A, showing unbiased $|F_o| - |F_c|$ electron density corresponding to G6P, contoured at 1 σ and coloured blue. The ring form of G6P is shown as cyan bonds and that of the straight chain as green bonds. Water molecules are represented as red spheres and potential hydrogen bonds are shown as broken lines. The proximity of Glu357 to carbon atoms 1 and 2 of G6P is denoted by broken lines. This Figure was prepared using Pymol (http://pymol.sourceforge.net/). (b) The contacts between PGI and the ring form of G6P. The distance between specific atoms are shown as broken lines and the distances are in Å. (c) Contacts between PGI and the straight-chain form of G6P.

the C1 and C2 hydroxyl groups are reversed. The C2 hydroxyl group of G6P and C1 hydroxyl group of F6P occupy similar positions, and both are within hydrogen-bonding distance of Glu357. Likewise, C1 of G6P is closer to C2 of F6P than C1. The respective ring oxygen atoms are positioned differently, but both are within hydrogen-bonding distance of His388. A water molecule in the rPGI-F6P complex occupies the same position as the C1 hydroxyl group in the open form of G6P. A water molecule occupies this position also when the ring form of G6P is present in the active site (see above).

Discussion

We have determined the crystal structure of mouse PGI in a sulphate-bound "native" form, bound to the inhibitor erythrose 4-phosphate, and in complex with its substrate molecule glucose-6-phosphate at 1.7 Å resolution. While the structure of rabbit PGI in complex with the cyclic form of the substrate, fructose-6-phosphate, is known,[8] this is the first structure of PGI bound with its other substrate, glucose 6-phosphate. In particular, the unique view of PGI of interacting with G6P, in both the ring and the straight-chain forms, provides new information regarding its enzyme mechanism.

Implications for catalytic mechanism

Phosphoglucose isomerase interconverts glucose 6-phosphate and fructose 6-phosphate. In solution, both of these substrates exist predominantly in their cyclic hemiacetal or hemiketal forms;[7] hence, it is assumed that PGI catalyzes two discrete activities; ring opening/closing, and the aldose/ketose isomerization itself. Crystal structures have implicated Glu357 as the base catalyst in the isomerization reaction,[5,6,18] and His388 as an acid catalyst in ring opening.[8,14] Mutational data of PGI from *Bacillus stearothermophilus* support a critical role for both of these residues in catalysis.[19,20]

Although His388 appears to be involved intimately in the ring-opening mechanism, another residue nearby is Lys518. In fact, in crystal

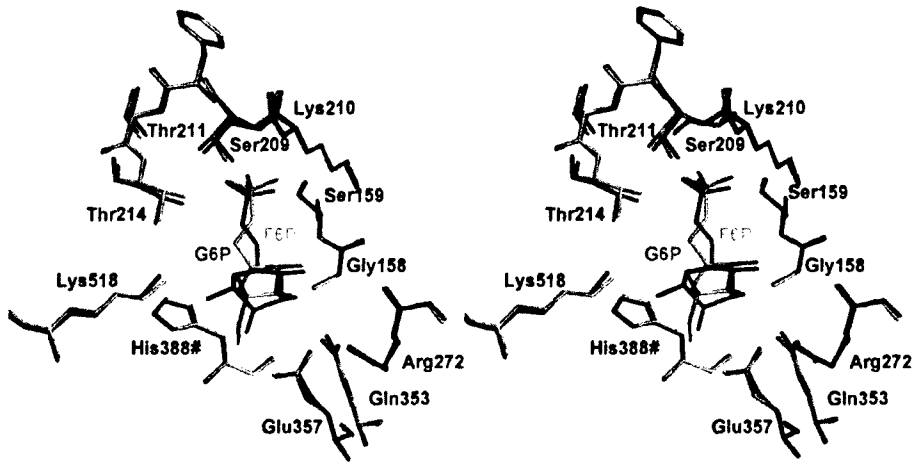

Figure 4. The structural overlap of active-site residues of PGI whether bound to G6P or F6P. This stereoview shows a superimposition of the active-site residues of mouse PGI in complex with G6P-bound (red bonds) and rabbit PGI in complex with F6P (yellow bonds).[8] For clarity, only the ring form of G6P is shown. This Figure was prepared using Pymol (http://pymol.sourceforge.net/).

structures of PGI in complex with 5-phosphoarabinonate (PAB)[6,10] (and in the complex with erythrose 4-phosphate presented here), Lys518 and His388 are equidistant from O4 (the equivalent atom in PAB to the substrate ring oxygen). In this situation, it remains possible that Lys518, and not His388, is the acid catalyst for ring opening. Fortunately, our high-resolution structure of mouse PGI in complex with G6P in both the straight-chain and the ring forms, resolves this ambiguity and clearly shows the role of Lys518 in catalysis. The relatively long distance (4.6 Å) between the amino group of Lys518 and the ring oxygen atom (of G6P in either the straight-chain form or the ring form) shows this residue is unlikely to abstract a proton from or donate a proton to O5, and that His388 is much better placed for this role. However, when the substrate is in its ring form, Lys518 forms a close contact with the C1 hydroxyl group, which suggests the primary role of this residue is to assist in ring opening by abstracting the C1 hydroxyl proton. It would participate in ring closure by donating the proton back to C1 (to form G6P) or C2 (to form F6P) and by positioning these groups near O5.

The complex of mouse PGI with G6P illuminates the conformational changes that the substrate undergoes during catalysis. Visualizing the substrate in both the ring form and the straight-chain form allows us to deduce the rearrangement that results in the transition from ring to straight and *vice versa*. It is clear that after ring opening, a simple rotation about the C3–C4 bond of the substrate is sufficient to swing the C1–C2 region to the opposite side of the active site, where it is brought into close proximity to the base catalyst, Glu357. No other rotation or perturbation to the substrate is required. This movement shows the clear spatial separation between the isomerase and ring opening/closing activities of PGI on opposite sides of the active site.

A comprehensive reaction mechanism

The new insight provided by the G6P-bound structure and, in particular, the role of Lys518 and the rotation of the substrate after ring opening, allows a detailed and comprehensive reaction scheme for PGI to be presented (Figure 5). After binding as a hemiacetal, the sugar ring of glucose 6-phosphate is opened in a concerted "push–pull" mechanism mediated by His388 and Lys518, in which the histidine residue protonates the C5 oxygen atom and the lysine residue simultaneously deprotonates the C1 hydroxyl group, forming the open-chain aldose. Rotation of the substrate about its C3–C4 bond then transports the C1–C2 region to a pocket formed by Gln511, Gly271, Arg272 and Glu357, where isomerization takes place. In this step, Glu357 abstracts the C2 proton and the resulting flow of electrons generates a double bond between C1 and C2, thus forming a *cis*-enediolate intermediate. The negative charge on this intermediate is stabilized by the positive charge of Arg272 and can resonate between the O1 and O2 positions. The outcome of the reaction depends on where Glu357 re-donates its proton. If it goes back to C2, then G6P is reformed, but if it is donated instead to C1, the C2 hydroxyl group loses a proton to form a ketone, and the open-chain ketose, F6P, is the product. As a prelude to ring closure, the C3–C4 bond rotates again to bring the C2 carbonyl group to within bonding distance of O5 and close to Lys518. Ring closure is the reverse of the push–pull ring-opening mechanism. Lys518 donates a proton to the C2 carbonyl oxygen atom and His388, now acting as a base, deprotonates the C5 oxygen atom, generating a short lived oxyanion that attacks the electron-deficient carbon centre at C2, thus forming the hemiketal product.

This mechanism fits well with all the structural evidence, but is less easy to reconcile with the pH

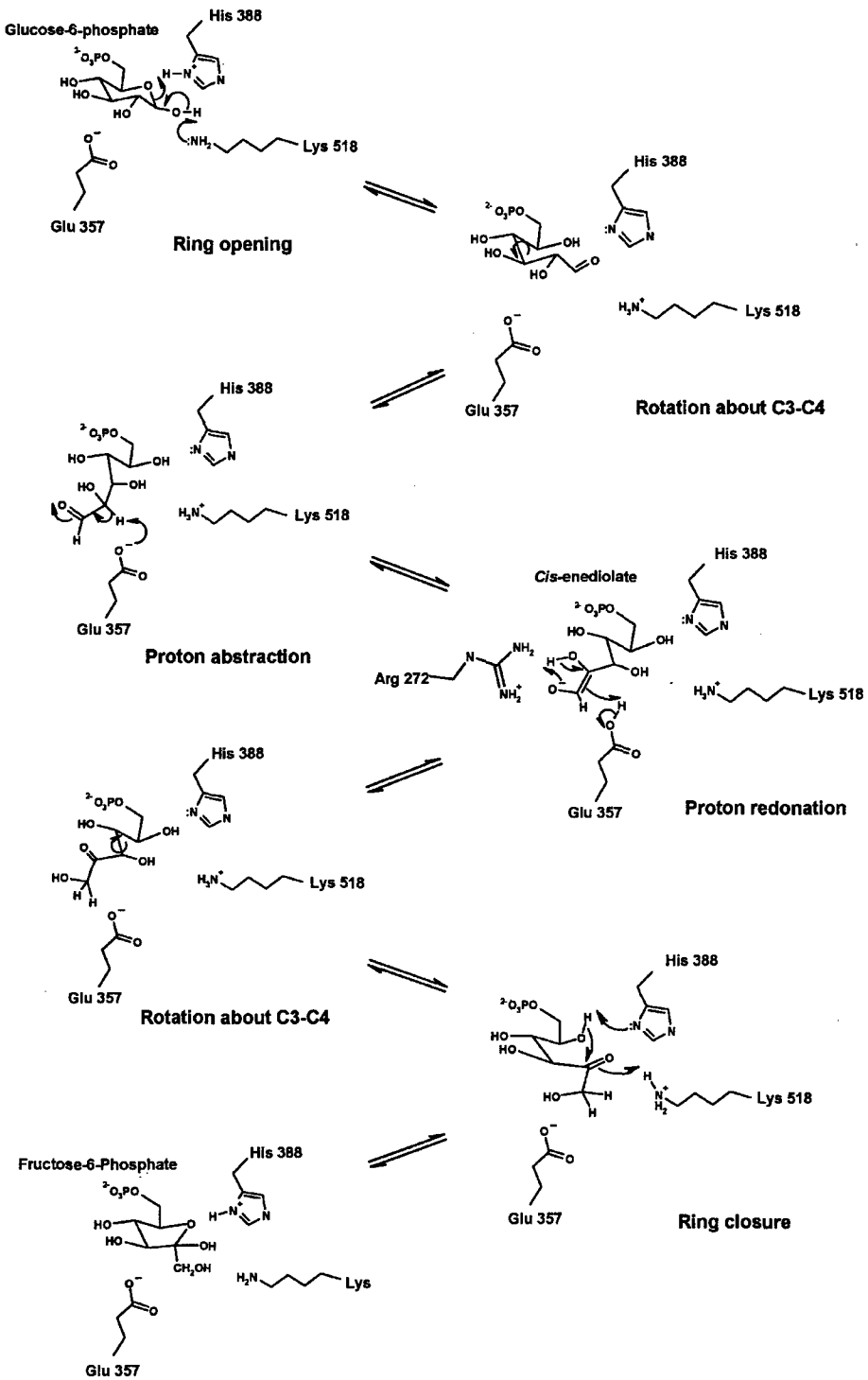

Figure 5. A comprehensive reaction mechanism for phosphoglucose isomerase. This scheme illustrates the critical role of Lys518 in ring opening and ring closing, as well as the rotation about the C3–C4 bond of the substrate that is required to bring C1–C2 (the site of proton transfer) alongside the base catalyst, Glu357. See the text for details.

profile of the reaction catalyzed by PGI.[21] This shows two transitions, at approximately pH 6.7 and pH 9.3; prior to the publication of any crystal structure of PGI, these were attributed to a histidine residue and a lysine residue, respectively. Similar pK_a values have been measured in PGI from different sources including yeast, rabbit and trypanosomes.[22,23] In agreement, our mechanism shows

the ionization of both a histidine residue and a lysine residue but, in apparent disagreement, that also of a third group, namely Glu357. Worse still, neither of the observed pK_a values fits well with the ionization of a glutamic acid residue, whose unperturbed pK_a is close to 4, and yet it is clear from the crystal structures of PGI that Glu357 is the base catalyst for isomerization. The best explanation is that the protein structure surrounding Glu357 perturbs the pK_a of this group upward toward neutrality, where its pK_a overlaps with that of His388 so that, in the pH profile, these two ionizations appear as one.

Conformational changes

A number of conformational changes that arise after PGI binds various inhibitor molecules have been described.[5,14,17] These comprise a closure of the small domain toward the sugar phosphate group, a small inward shift of the 3_{10} helix (residues 383–389) that carries His388, and the movement of helix α23 (residue 512–522), which brings Lys518 closer to the active site. In the structure of mouse PGI, solved in the absence of inhibitor or substrate molecules, the shift in the small domain has occurred only in molecule A in response to the binding of a sulphate ion at the sugar phosphate-binding site. Two sulphate ions are present in molecule B but none overlaps with the phosphate-binding position and hence the conformation of the small domain is open. In common with other inhibitor complexes of PGI,[6,10] all three structural changes are observed in the crystal structure of mouse PGI complexed with E4P. The situation in the complex with G6P, however, is more complicated.

The active site of molecule B of the complex with G6P is apparently devoid of substrate, but a sulphate ion now occupies the phosphate-binding site. Interestingly, this sulphate ion does not induce the expected closure of the small domain and molecule B remains in the open state (not shown). Close examination of the difference $|F_o|-|F_c|$ density in this region, however, shows numerous peaks of positive density in the loops that normally shift in the small domain, all of which lie nearer the active site than the current placement of the protein chain, and is evidence that some conformational changes are occurring. Clearly then, in molecule B, there exists a mixed population of open and closed forms with the open form dominating. At first sight, this might suggest some communication between the two subunits in the dimer, in which G6P binding to molecule A leads to a slight change in the conformation of molecule B and so increases affinity for sulphate at the phosphate-binding site. A better explanation, though, is that the two peaks of electron density in the active site of molecule B attributed to sulphate ions are actually due to G6P bound with low occupancy. It is unclear why this subunit apparently has a lower affinity for G6P compared to molecule A, but it may be due to the different crystal packing around this subunit. E4P was able to bind to molecule B because of its much higher affinity compared to G6P (K_i in the micromolar range *versus* K_m in the millimolar range).

When molecule A of the G6P complex is compared to molecule A of the substrate-free "native" structure, none of the conformational changes has occurred: the small domain is already in the closed form (due to the presence of sulphate in the native structure), likewise the 3_{10} helix carrying His388 has not moved significantly, and α23 remains in its native position, further away from the active site. The same view as molecule A is seen in the complex of rabbit PGI with F6P in its ring form.[8] The movement of α23 cannot be constrained by crystal packing interactions, because it has shifted in the complex with E4P. One explanation for this configuration is that α23 shifts toward the active site only when the substrate is present in the straight-chain form, i.e. after ring opening and after rotation of the C3–C4 bond. However, this is unlikely because the complex of PGI with G6P contains a mixture of substrate in both ring and straight-chain forms. Another explanation is that the movement in α23 occurs only when PGI binds inhibitors (e.g. E4P as noted above) and does not occur during the normal catalytic reaction involving F6P or G6P. To prove or disprove this hypothesis would require a structure of PGI in complex with substrate present wholly in the straight-chain form. Nonetheless, it is interesting to note the lack of structural difference between mouse PGI in complex with G6P and rabbit PGI in complex with ring-form F6P (Figure 4),[8] which suggests that perhaps the conformational changes in PGI arise directly from the binding of substrate but, once bound, the only movements associated with catalysis are of the substrate itself.

Why conventional PGIs do not catalyse a phosphomannose isomerase activity

One of the more exquisite features of PGI is its ability to isomerize glucose 6-phosphate to fructose 6-phosphate but not mannose 6-phosphate to the same product. A very slight phosphomannose (PMI) activity has been measured in the yeast enzyme,[11] but at a non-physiological rate. G6P and M6P are epimers and differ only in the configuration at C2. Interestingly, PGI does bind M6P and catalyzes the interconversion of its anomeric forms.[24] How then does PGI prevent the isomerisation of M6P to F6P? The structure of mouse PGI in complex with glucose 6-phosphate in both the straight-chain form and the ring form provides an ideal framework with which to answer this question. As this structure shows, after the ring-opening step, a rotation about the C3–C4 bond brings the C1–C2 region of G6P (or F6P) into proximity with the base catalyst, Glu357. We modeled the straight-chain form of M6P into the active site of PGI using the straight-chain form of G6P as a template. M6P could be positioned so that the proton to be

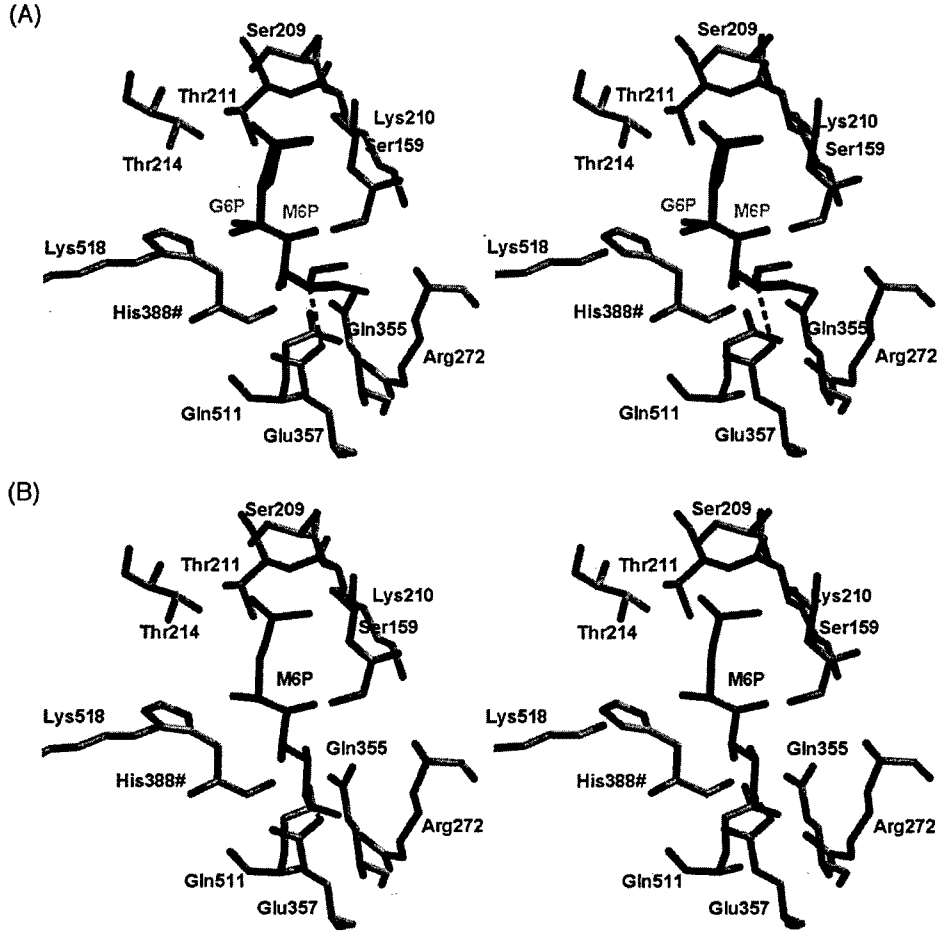

Figure 6. The structural basis for the specificity of PGI for glucose 6-phosphate over mannose 6-phosphate. In this stereoview, (A) shows the active-site region of mouse PGI in complex with the straight-chain form of G6P (coloured orange). The model of straight-chain mannose 6-phosphate (coloured green) is shown superimposed onto G6P such that the proton at C2 is directed toward Glu357. To form F6P, any proton abstracted from C2 of M6P must be donated back to C1. For C1 to reach Glu357, however, requires a rotation of M6P about its C2–C3 bond and this leads to a steric clash of the C1 hydroxyl group of M6P with Gln511, as shown in (B).

abstracted from C2 was pointing toward the base catalyst, Glu357, suggesting that, at least, abstraction of this proton is possible in PGI. But, in order for the proton to be donated back to C1, M6P must undergo rotation about the C2–C3 bond[11] to position C1 near Glu357. Rotation in one direction is prevented by a clash between the C2 hydroxyl group and Glu357 (clockwise about the C3–C2 bond, viewed from C3). Rotation in the opposite direction is impeded due to a steric clash between C1–O1 and the side-chain of Gln511 (Figure 6). This glutamine residue is highly conserved within the PGI family of enzymes and lies immediately adjacent to Glu357. If O1 were moved to a position *trans* to O2 through rotation about C1–C2, rotation of C2–C3 would be prevented by a clash with Gln353 (not shown). Thus, it seems likely that Gln511 and, to a lesser extent, Gln353, constitutes the structural basis for the specificity of PGI for G6P over M6P. Distantly related members of the PGI superfamily in Archaeal species such as *Aeropyrum pernix* and *Thermoplasma acidophilum* function as bifunctional PGI/PMI enzymes.[12] It will be interesting to determine whether the active sites of these enzymes permit such a rotation about C2–C3 and so isomerize M6P to F6P.

Materials and Methods

Protein expression and purification

A full-length mouse cDNA was identified by searching the NCBI database of EST clones, using the original sequence entry (Genbank accession no. M14220, mouse neuroleukin). A cDNA corresponding to Genbank accession number AI037338 was obtained from the IMAGE Consortium, and a 1.7 kb DNA fragment encoding only the open reading frame was prepared by PCR as described for rabbit PGI.[25] Flanking PCR primers changed the 5′ end to a methionine start codon within a

unique NdeI restriction enzyme recognition site, and the normal stop codon was replaced by six histidine codons followed by a new UAA stop codon plus an EcoRI recognition site. The PCR primers were used to amplify the open reading frame with a minimal cycle number and high-fidelity Vent DNA polymerase (NE BioLabs Inc). The amplified DNA was subcloned into the bacterial expression vector pET5a as an NdeI-to-EcoRI fragment and expressed in *Escherichia coli* BL21DE3pLysS (Stratagene Inc). Bacteria were induced with 0.5 mM isopropyl-β,D-thiogalactopyranoside (IPTG) for three hours at 30 °C. Cell pellets were collected by low-speed centrifugation, lysed by sonication without protease inhibitors, and clarified by high-speed centrifugation. Soluble supernatants were bound to Ni-NTA agarose (Qiagen Inc.) and washed and eluted according to the manufacturer's standard protocol. The material eluting in 0.25 M imidazole was >95% homogenous as estimated from Coomassie blue staining of the protein on denaturing, reducing 12.5% (w/v) polyacrylamide gels. Yields were 25–50 mg per liter of bacterial culture. The purified protein was concentrated to approximately 4 mg/ml and equilibrated with phosphate-buffered standard saline using Centricon-30 ultrafiltration (Amicon Inc).

When the inserted DNA within the expression vector was sequenced, two differences were noted from the canonical sequence (Genbank accession no. M14220) of mouse neuroleukin. The first was D94N (codon at nucleotides 315–317 changed from GAT to AAT). The second was F263L (codon at nucleotides 842–844 changed from TTC to TTA). The first change corresponds to a common polymorphism that defines the Gpi1-Sa *versus* Gpi-Sb alleles, which are used as a routine electrophoretic marker in mouse gene mapping.[26] The second alteration is unusual and did not occur in 50 additional mouse EST, expressed sequence tag (EST) sequences that cover this region. The F263L protein was stable and enzymatically active (not shown). We verified the sequence variant in a second sample of the IMAGE cDNA, which was constructed from C57BL/6J male mouse mammary gland RNA. It is unclear whether this is a rare natural polymorphism or a cloning artifact.

Crystallization and data collection

The protein was subjected to crystallization trials using the hanging-drop method. Crystals of mPGI were cryofrozen by passing through a stabilizing solution of 1.9 M ammonium sulphate, 100 mM Tris–HCl (pH 8.5), with glycerol added to 30% (v/v) final concentration as cryoprotectant. Diffraction data were collected on a RAXIS-IV++ imaging plate system mounted on an RU-H3R X-ray generator operating at 50 kV and 100 mA and fitted with Osmic Confocal Optics (Rigaku/MSC, The Woodlands, TX). The crystal-to-detector distance was 100 mm and 414° of data were collected in 0.5° oscillations with an exposure time of eight minutes per frame.

To introduce substrate or inhibitor molecules, the crystals were soaked in stabilizing solutions containing the ligand. The complex with glucose 6-phosphate arose following a soak in fructose 6-phosphate. Molarities of ligand and the soaking times were varied to ensure maximal occupancy of the active site, as judged by difference Fouriers after refinement of the model against that data set. The crystals were cryoprotected as before, using 30% glycerol. Typically, 200° of data were collected to obtain essentially complete data sets. The data set collected from a crystal soaked in erythrose 4-phosphate was collected on the home source (as above) and processed with CrystalClear.[27] The data collected from the crystal soaked in fructose 6-phosphate were collected at beamline 22 at the Advanced Photon Source. For this experiment, the crystal-to-plate distance was 130 mm, the exposure time was one second and 360° data were acquired using a MAR225 CCD system. These data were processed using d*Trek.[27]

Structure determination

The structure of mouse PGI was solved by molecular replacement using a dimer of rabbit PGI[14] as a search model. The calculation was performed using MOLREP[28] and used data extending to 3 Å resolution. A single clear solution arose with an *R*-factor of 37.6% and correlation coefficient of 0.65. This solution was then applied to a homology model of mouse PGI, which had been generated from the rabbit structure using the Swiss-Model Server.[29] After an initial refinement using XPLOR,[30] the model was improved by iterative cycles of manual rebuilding, using O,[31] and crystallographic refinement with REFMAC.[32] 5% of reflections were set aside from the refinement and used to calculate the R_{free}. Molecules of water, glycerol, sulphate and β-mercaptoethanol were added if visible in both $|F_o|-|F_c|$ and $2(|F_o|-|F_c|)$ electron density maps and if within hydrogen bonding distance of at least two other atoms in the structure. Water modeling was performed using ARP/wARP.[33] When PGI is purified from rabbit, the N-terminal residue is alanine.[34] Although this construct of PGI contains a methionine residue at the N terminus, neither of these is visible in the electron density map, and so in accordance with the native protein, the final structure is numbered 1–557, starting at Ala1.

For the ligand-bound structures, the starting model for refinement was the sulphate-bound native structure. After initial refinement, each ligand was modeled into its respective $|F_o|-|F_c|$ density and thereafter the procedure for refinement was the same as for the native structure. To generate unbiased electron density for pictures showing the binding of ligands to the active site of PGI, an additional round of refinement was performed in which the occupancies of those ligands was set to zero. The O program was used to model mannose 6-phosphate into mouse PGI and to perform rotations of the molecule within the active site.

Protein Data Bank accession codes

The coordinates and structure factors for each structure have been submitted to the RCSB Protein Data Bank (PDB): code Native, 1U0E; E4P, 1U0F, F6P, 1U0G.

Acknowledgements

J.T.G.S. is supported by a grant from the National Science Foundation (EPS-0132573) and E.M.Z. is supported by a cross-training grant from the NIH (R25GM067084). This research was supported also by grants from the U.S. Army (DAMD17-98-1-8245 and DAMD17-02-1-0586) to J.M.C. We extend our gratitude to Klaus Schnackerz, whose gift of 5-phosphoarabinonate has greatly assisted our ongoing studies of PGI. Data were collected at the Southeast Regional Collaborative Access Team

(SER-CAT) 22-ID beamline at the Advanced Photon Source, Argonne National Laboratory. Supporting institutions may be found at www.ser-cat.org/members.html. Use of the Advanced Photon Source was supported by the U.S. Department of Energy, Office of Science, Office of Basic Energy Sciences, under contract no. W-31-109-Eng-38.

References

1. Gurney, M. E., Apatoff, B. R., Spear, G. T., Baumel, M. J., Antel, J. P., Bania, M. B. & Reder, A. T. (1986). Neuroleukin: a lymphokine product of lectin-stimulated T cells. *Science*, **234**, 574–581.
2. Watanabe, H., Takehana, K., Date, M., Shinozaki, T. & Raz, A. (1996). Tumor cell autocrine motility factor is the neuroleukin/phosphohexose isomerase polypeptide. *Cancer Res.* **56**, 2960–2963.
3. Xu, W., Seiter, K., Feldman, E., Ahmed, T. & Chiao, J. W. (1996). The differentiation and maturation mediator for human myeloid leukemia cells shares homology with neuroleukin or phosphoglucose isomerase. *Blood*, **87**, 4502–4506.
4. Rose, I. A. (1975). Mechanism of the aldose-ketose isomerase reactions. *Advan. Enzymol. Relat. Areas Mol. Biol.* **43**, 491–517.
5. Read, J., Pearce, J., Li, X., Muirhead, H., Chirgwin, J. & Davies, C. (2001). The crystal structure of human phosphoglucose isomerase at 1.6 Å resolution: implications for catalytic mechanism, cytokine activity and haemolytic anaemia. *J. Mol. Biol.* **309**, 447–464.
6. Jeffery, C. J., Hardre, R. & Salmon, L. (2001). Crystal structure of rabbit phosphoglucose isomerase complexed with 5-phospho-D-arabinonate identifies the role of Glu357 in catalysis. *Biochemistry*, **40**, 1560–1566.
7. Swenson, C. A. & Barker, R. (1971). Proportion of keto and aldehyde forms in solutions of sugars and sugar phosphates. *Biochemistry*, **10**, 3151–3154.
8. Lee, J. H., Chang, K. Z., Patel, V. & Jeffery, C. J. (2001). Crystal structure of rabbit phosphoglucose isomerase complexed with its substrate D-fructose 6-phosphate. *Biochemistry*, **40**, 7799–7805.
9. Jeffery, C. J., Bahnson, B. J., Chien, W., Ringe, D. & Petsko, G. A. (2000). Crystal structure of rabbit phosphoglucose isomerase, a glycolytic enzyme that moonlights as neuroleukin, autocrine motility factor, and differentiation mediator. *Biochemistry*, **39**, 955–964.
10. Davies, C., Muirhead, H. & Chirgwin, J. (2003). The structure of human phosphoglucose isomerase complexed with a transition-state analogue. *Acta Crystallog. sect. D*, **59**, 1111–1113.
11. Seeholzer, S. H. (1993). Phosphoglucose isomerase: a ketol isomerase with aldol C2-epimerase activity. *Proc. Natl Acad. Sci. USA*, **90**, 1237–1241.
12. Hansen, T., Wendorff, D. & Schonheit, P. (2004). Bifunctional phosphoglucose/phosphomannose isomerases from the Archaea *Aeropyrum pernix* and *Thermoplasma acidophilum* constitute a novel enzyme family within the phosphoglucose isomerase superfamily. *J. Biol. Chem.* **279**, 2262–2272.
13. Matthews, B. (1968). Solvent content of protein crystals. *J. Mol. Biol.* **33**, 491–497.
14. Davies, C. & Muirhead, H. (2003). The crystal structure of native phosphoglucose isomerase from rabbit: conformational changes associated with catalytic function. *Acta Crystallog. sect. D*, **59**, 453–465.
15. Davies, C. & Muirhead, H. (2002). The crystal structure of phosphoglucose isomerase from pig muscle and its complex with 5-phosphoarabinonate. *Proteins: Struct. Funct. Genet.* **49**, 577–579.
16. Chirgwin, J. M., Parsons, T. F. & Noltmann, E. A. (1975). Mechanistic implications of the pH independence of inhibition of phosphoglucose isomerase by neutral sugar phosphates. *J. Biol. Chem.* **250**, 7277–7279.
17. Arsenieva, D. & Jeffery, C. (2002). Conformational changes in phosphoglucose isomerase induced by ligand binding. *J. Mol. Biol.* **323**, 77–84.
18. Davies, C. (1991). The three-dimensional structure of glucose 6-phosphate isomerase, PhD thesis, University of Bristol.
19. Meng, M., Chane, T. L., Sun, Y. J. & Hsiao, C. D. (1999). Probing the location and function of the conserved histidine residue of phosphoglucose isomerase by using an active site directed inhibitor N-bromoacetylethanolamine phosphate. *Protein Sci.* **8**, 2438–2443.
20. Meng, M., Lin, H.-Y., Hsieh, C.-J. & Chen, Y.-T. (2001). Functions of the conserved anionic amino acids and those interacting with substrate phosphate group of phosphoglucose isomerase. *FEBS Letters*, **499**, 11–14.
21. Dyson, J. E. D. & Noltmann, E. A. (1968). The effect of pH and temperature on the kinetic parameters of phosphoglucose isomerase. Participation of histidine and lysine in a proposed dual function mechanism. *J. Biol. Chem.* **243**, 1401–1414.
22. O'Connell, E. L. & Rose, I. A. (1973). Affinity labeling of phosphoglucose isomerase by 1,2-anhydrohexitol-6-phosphates. *J. Biol. Chem.* **248**, 2225–2231.
23. Marchand, M., Kooysra, U., Wierenga, R. K., Lambier, A. M., van Beeuman, J., Opperdoes, F. R. & Michels, P. A. M. (1989). Glucosephosphate isomerase from *Trypanosoma brucei*. Cloning and characterization of the gene and analysis of the enzyme. *Eur. J. Biochem.* **184**, 455–464.
24. Rose, I. A., O'Connell, E. L. & Schray, K. J. (1973). Mannose 6-phosphate: anomeric form used by phosphomannose isomerase and its 1-epimerization by phosphoglucose isomerase. *J. Biol. Chem.* **248**, 2232–2234.
25. Li, X. & Chirgwin, J. M. (2000). Rabbit phosphoglucose isomerase/neuroleukin/autocrine motility factor: cloning *via* interspecies identity. *Biochim. Biophys. Acta*, **1476**, 363–367.
26. Pearce, S. R., Morgan, M. J., Ball, S., Peters, J. & Faik, P. (1995). Sequence characterization of alleles Gpi1-Sa and Gpi1-Sb at the glucose phosphate isomerase structural locus. *Mamm. Genome*, **6**, 537–539.
27. Pflugrath, J. W. (1999). The finer things in X-ray diffraction data collection. *Acta Crystallog. sect. D*, **55**, 1718–1725.
28. Vagin, A. & Teplyakov, A. (1997). MOLREP: an automated program for molecular replacement. *J. Appl. Crystallog.* **30**, 1022–1025.
29. Peitsch, M. C. (1996). ProMod and Swiss-Model: Internet-based tools for automated comparative protein modelling. *Biochem. Soc. Trans.* **24**, 274–279.
30. Brünger, A. T. (1992). *X-PLOR. Version 3.1, A System for X-ray Crystallography and NMR*. Yale University, New Haven, CT.
31. Jones, T. A., Zou, J.-Y., Cowan, S. W. & Kjeldgaard, M. (1991). Improved methods for building protein structures in electron-density maps and the location of errors in these models. *Acta Crystallog. sect. A*, **47**, 110–119.
32. Murshudov, G. N., Vagin, A. A. & Dodson, E. J. (1997).

Refinement of macromolecular structures by the maximum-likelihood method. *Acta Crystallog. sect. D*, **53**, 240–255.
33. Perrakis, A., Harkiolaki, M., Wilson, K. S. & Lamzin, V. S. (2001). ARP/wARP and molecular replacement. *Acta Crystallog. sect. D*, **57**, 1445–1450.
34. James, G. T. & Noltmann, E. A. (1972). Chemical studies on the subunit structure of rabbit muscle phosphoglucose isomerase. *J. Biol. Chem.* **248**, 730–737.
35. Kraulis, P. J. (1991). MOLSCRIPT: a program to produce both detailed and schematic plots of protein structures. *J. Appl. Crystallog.* **24**, 946–950.
36. Merritt, E. A. & Bacon, D. J. (1997). Raster3D: photorealistic molecular graphics. *Methods Enzymol.* **277**, 505–524.

Edited by I. Wilson

(Received 26 May 2004; received in revised form 19 July 2004; accepted 23 July 2004)